HHS Public Access

Author manuscript

*Nature*. Author manuscript; available in PMC 2021 February 19.

Published in final edited form as:

*Nature*. 2020 September ; 585(7823): 96–101. doi:10.1038/s41586-020-2625-x.

# C9orf72 in myeloid cells suppresses STING-induced inflammation

**Madelyn E. McCauley**[1,2], **Jacqueline Gire O'Rourke**[1,2], **Alberto Yáñez**[7], **Janet L. Markman**[4], **Ritchie Ho**[2], **Xinchen Wang**[6], **Shuang Chen**[4], **Deepti Lall**[1,2], **Mengyao Jin**[4,5], **A.K.M.G Muhammad**[1,2], **Shaughn Bell**[1,2], **Jesse Landeros**[1], **Viviana Valencia**[1], **Matthew Harms**[6], **Moshe Arditi**[4], **Caroline Jefferies**[4,5], **Robert H. Baloh**[1,2,3,*]

[1]Center for Neural Science and Medicine, Division of Rheumatology Cedars-Sinai Medical Center, 8700 Beverly Blvd, Los Angeles, CA 90048, USA.

[2]Regenerative Medicine Institute, Division of Rheumatology Cedars-Sinai Medical Center, 8700 Beverly Blvd, Los Angeles, CA 90048, USA.

[3]Department of Neurology, Division of Rheumatology Cedars-Sinai Medical Center, 8700 Beverly Blvd, Los Angeles, CA 90048, USA.

[4]Department of Biomedical Sciences, Division of Rheumatology Cedars-Sinai Medical Center, 8700 Beverly Blvd, Los Angeles, CA 90048, USA.

[5]Department of Medicine, Division of Rheumatology Cedars-Sinai Medical Center, 8700 Beverly Blvd, Los Angeles, CA 90048, USA.

[6]Institute for Genomic Medicine, Columbia University, 710 West 168th St, New York, NY 10032

[7]Departament de Microbiologia i Ecologia, Universitat de València, Burjassot, Spain

Amyotrophic lateral sclerosis (ALS) and frontotemporal dementia (FTD) are neurodegenerative disorders which overlap in their clinical presentation, pathology, and



* robert.baloh@csmc.edu.

Estructura de Recerca Interdisciplinar en Biotecnologia i Biomedicina, Universitat de València, Burjassot, Spain

**Author Contributions** M.E.M. coordinated the project, was involved in all experiments, as well as data collection and statistical analysis. J.G.O., J.L., M.E.M. were involved in EAE experiments. M.E.M. and A.Y. performed flow cytometry. J.G.O., V.V., and M.E.M. were involved in BMDM, PBMC, and MDM experiments and analysis. V.V. and J.G.O. performed western blots. J.L.M., S.C. and M.A. were involved in B16 melanoma experiments and analysis. A.K.M.G.M. performed H&E and LFB staining. D.L. performed microglia experiment and analysis. J.L. established and maintained mouse colonies. A.K.M.G.M., J.G.O., M.E.M. performed tissue collections and analysis. S.B., R.H., X.W., M.H., analyzed RNA-seq data. M.E.M., C.J. and R.H.B. planned, designed, and interpreted the experiments. M.E.M. and R.H.B. wrote the manuscript.

**Data Availability Statement.** The accession numbers for the RNA sequencing data reported in this paper are Gene Expression Omnibus (GEO): GSE151936. Data from GSE151936 was used for Figure 1h,i, Figure 2k, Figure 4a,b,i, Extended Data Figure 4a,b, Extended Data 5a,b, Extended Data 6a–g, Extended Data 7c, Extended Data 8a–f. Human whole blood RNA sequencing data reported in this paper can be accessed on dbGaP with accession: phs002055.v1.p1. Data from dbGaP with accession: phs002055.v1.p1 was used for Figure 4d,e. Human cerebellum RNA-seq data can be found Prudencio, M. *et al.*

**Human Research Participants.** All human research (collection of blood from subjects with ALS or normal controls) was performed with informed consent, according to protocols approved by the institutional review boards of Cedars-Sinai Medical Center (IRB # Pro00039304), or Columbia University Medical Center (IRB-AAAQ7026).

Competing interests

The authors declare no competing interests.

genetic origin. An over-representation of autoimmune disorders exists in both ALS and FTD, but this remains an unexplained epidemiologic observation[1–3]. Expansions of a hexanucleotide repeat (GGGGCC) in the *C9orf72* gene are the most common cause of familial ALS and FTD (C9-ALS/FTD), leading to both repeat containing RNA and dipeptide accumulation coupled with decreased C9orf72 protein expression in brain and peripheral blood cells[4–6]. Here we show that loss of *C9orf72* in myeloid cells is sufficient to recapitulate the age dependent lymphoid hypertrophy and autoinflammation seen in complete *C9orf72*$^{-/-}$ mice. Dendritic cells isolated from *C9orf72*$^{-/-}$ mice showed marked early activation of the type I interferon response, and *C9orf72*$^{-/-}$ myeloid cells were selectively hyperresponsive to activators of STING, a key regulator of the innate immune response to cytosolic DNA. STING degradation through the autolysosomal pathway was diminished in *C9orf72*$^{-/-}$ myeloid cells, and blocking STING suppressed hyperactive type I interferon responses in *C9orf72*$^{-/-}$ immune cells, splenomegaly and inflammation in *C9orf72*$^{-/-}$ mice. Additionally, mice lacking one or both copies of *C9orf72* were more susceptible to experimental autoimmune encephalitis, mirroring the susceptibility to autoimmune diseases seen in C9-ALS/FTD patients. Finally, we found that blood derived macrophages, whole blood, and brain tissue from C9-ALS/FTD patients all showed an elevated type I interferon signature compared to sporadic ALS/FTD subjects that could be suppressed with a STING inhibitor. Collectively, our results suggest that C9-ALS/FTD patients have an altered immunophenotype due to loss of C9orf72 suppression of STING/type I interferon mediated inflammation.

*C9orf72* knockout mice demonstrate lymphoid organ hyperplasia and age-related systemic inflammation, however depending on their environment they ranged from having no tissue injury and a normal lifespan[7], to autoantibody production with renal injury[8], or fatal spontaneous autoimmune disease[9]. In the immune system, C9orf72 is most highly expressed in myeloid cells, especially dendritic cells[7]. Dendritic cells (DCs) are antigen presenting cells of the innate immune system that regulate the adaptive immune response, playing an important role in autoimmunity and cancer immunity[10,11]. To assess the affect of loss of C9orf72 in DCs, we analyzed the activation state of splenic DCs from *C9orf72*$^{-/-}$ mice at 8 weeks when minimal inflammation or lymphoid hyperplasia are present, and 8 months when the mice have pronounced markers of systemic inflammation (Extended Data Fig. 1). Although DC subtype development was normal in *C9orf72*$^{-/-}$ mice (Extended Data Fig. 1a), we observed increased costimulatory molecule (CD86) expression on CD11b+ DCs from *C9orf72*$^{-/-}$ mice, that became more prominent with age (Fig 1a,b). DCs are crucial for regulating T cell homeostasis, activation and tolerance, and T cells were previously reported to be activated in aged *C9orf72*$^{-/-}$ mice[8]. T cell development in the thymus was normal in *C9orf72*$^{-/-}$ mice (Extended Data Fig. 1f), however memory and effector memory CD4 and CD8 T cells were increased even at 8 weeks, and became more pronounced with age (Fig 1c,d). Given that *C9orf72* is also expressed at low levels in lymphocytes, we crossed mice containing a *C9orf72* conditional null allele (*C9orf72*$^{fl/fl}$)[12] to two different myeloid specific Cre driver lines, *Cx3cr1*$^{Cre}$ and *LysM*$^{Cre}$, to determine if the phenotype was cell autonomous to myeloid cells. The loss of *C9orf72* selectively in myeloid populations (primarily monocytes, tissue macrophages, and dendritic cells[13]) in *C9orf72*$^{fl/fl}$:*Cx3cr1*$^{Cre}$ mice completely recapitulated the splenomegaly, altered DC costimulatory molecule expression,

and T cell activation seen in *C9orf72* whole body knockout mice (Fig 1e,f, Extended Data Fig. 2c,d). Similar findings were observed in *C9orf72*$^{fl/fl}$:*LyzM*$^{Cre}$ mice (Extended Data Fig. 3), although to a milder degree potentially because the *LyzM*$^{Cre}$ driver is expressed in fewer dendritic cells (<10%) compared to the *Cx3cr1*$^{Cre}$ driver (>90%)[13]. To probe the non-cell autonomous phenotypes of adaptive immune cells further, we sorted splenocyte populations from control, *C9orf72*$^{-/-}$, and *C9orf72*$^{fl/fl}$:*Cx3cr1*$^{Cre}$ mice. Pathway analysis of CD4 and CD8 T cells from *C9orf72*$^{fl/fl}$:*Cx3cr1*$^{Cre}$ mice showed selective upregulation of type I interferon signaling, suggesting that these cells were responding to type I interferons produced by myeloid cells (Fig 1g–i; Extended Data Fig 4).

To better characterize the drivers of activation of adaptive immune cells by *C9orf72* deficient DCs, we performed RNA-sequencing on isolated splenic classical DCs (cDCs) from young wildtype and *C9orf72*$^{-/-}$ mice. Principle component analysis (PCA) showed separation of the two genotypes, with *C9orf72*$^{-/-}$ DCs having increased expression of a variety of inflammatory cytokines including IL6, IL10 and IL12β (Extended Data Fig 5a,b). Heat map analysis with hierarchical clustering confirmed strong upregulation of canonical type I interferon response genes in *C9orf72*$^{-/-}$ DCs in three of four animals, with no apparent difference in NFκB signaling (Fig. 2a,b). To identify the potential drivers of the hyperactive type I interferon response, we cultured wildtype and *C9orf72*$^{-/-}$ bone marrow derived macrophages (BMDMs) and stimulated them with several toll-like and cytosolic receptor agonists. Activation of Tlr3, Tlr4 and Tlr7 signaling showed similar IFNβ production between wildtype and *C9orf72*$^{-/-}$ BMDMs (Extended Data Fig. 5c–e). However, stimulation with cGAMP, an agonist of the cGAS-STING pathway for sensing cytosolic double stranded DNA[14], showed a hyperactive response in IFNβ and interferon stimulated gene (ISG) production in *C9orf72*$^{-/-}$ BMDMs compared to wildtype BMDMs (Fig. 2c–e). STING signaling is regulated by trafficking to the lysosome, and blocking autophagy leads to sustained activation of the type I interferon response and inflammation[15–17]. Given that C9orf72 is involved in endosomal trafficking, autophagy and lysosomal function[18], we hypothesized that STING degradation was disrupted in *C9orf72*$^{-/-}$ cells. Indeed, we observed delayed degradation of STING after stimulation with cGAMP, and persistence of S365 phospho-STING in *C9orf72*$^{-/-}$ BMDMs (Fig. 2f,g), indicating more STING was present to promote IFN activation via IRF3, and that it was marked for lysosomal degradation. Basal LC3-II levels in *C9orf72*$^{-/-}$ BMDMs were increased compared to controls, and we observed that the recently reported induction of LC3-II lipidation by cGAMP activation of STING[19] was further increased in *C9orf72*$^{-/-}$ BMDMs (Fig 2h). This difference was normalized by treatment with bafilomycin A1, suggesting that it was driven in part by decreased lysosomal degradation of LC3-II in C9orf72 deficient cells (Fig 2h). These data support a model whereby diminished lysosomal degradation of STING through autophagy leads to increased STING in late endosomes serving as a platform for persistent IFN induction[19]. In support of this idea, the hyperactive IFNβ induction by C9orf72 BMDMs to cGAMP was completely blocked by a STING antagonist[20] (Fig 2i). To further determine to what degree the elevated type I IFN signature in *C9orf72*$^{-/-}$ mice was driven by STING in vivo, we crossed *C9orf72*$^{-/-}$ mice to STING deficient *goldenticket* mice (STING$^{gt/gt}$). We observed a rescue of splenomegaly and the myeloid activation marker (Trem2) in *C9orf72*$^{-/-}$;STING$^{gt/gt}$ mice compared to *C9orf72*$^{-/-}$ mice (Fig. 2j,k). To further

characterize the rescue we performed RNA-seq on splenocytes from wildtype, *C9orf72*$^{-/-}$ and *C9orf72*$^{-/-}$;STING$^{gt/gt}$ mice. We observed that the elevated type I IFN response in isolated splenic CD11b myeloid cells, B cells, CD4 and CD8 T cells was completely rescued by the deletion of STING (Fig 2l, Extended Data Fig 6). In contrast, myeloid and T cell activation markers were not fully rescued in the *C9orf72*$^{-/-}$;STING$^{gt/gt}$ mice (Extended Data Fig 7). The lack of full rescue of systemic inflammatory phenotypes in *C9orf72*$^{-/-}$;STING$^{gt/gt}$ mice may be because STING deletion itself promotes hyperactive TLR signaling and inflammation[21], or because C9orf72 can also regulate non-STING related pathways[22]. Regardless, these findings support that increased STING activity in *C9orf72*$^{-/-}$ myeloid cells drives the chronically elevated type I interferon production observed in these cells, and is a key part of the systemic autoinflammation in *C9orf72*$^{-/-}$ mice.

We observed strong expression of IL12β from *C9orf72*$^{-/-}$ dendritic cells (Extended Data Fig 5b), which together with IFN-α/β can promote Th1 T cell polarization[23], and this was supported by increased IL2 and IFNγ in stimulated splenic T cells from *C9orf72*$^{-/-}$ mice (Extended Data Fig. 1h), and RNA-seq of isolated splenic T cells which showed elevation of markers of activation and Th1 polarization (Extended Data Fig 8). There was also a nonsignificant trend toward elevated IL17, which drives production of Th17 cells (Extended Data Fig. 8). This supports that activation of adaptive immune cells from chronic STING/type I IFN in *C9orf72*$^{-/-}$ mice leads to the propensity to develop autoimmune disease, similar to chronic STING activation in mice lacking Trex1[24]. We therefore asked if *C9orf72*$^{-/-}$ mice in our colony, which demonstrate autoinflammation without spontaneous autoimmune disease, were more susceptible to experimental autoimmune encephalitis (EAE), which has a strong Th1 and Th17 T cell component[25]. We observed a graded gene dose-dependent increase in clinical severity and spinal cord inflammation in mice lacking either one or both copies of *C9orf72* (Fig 3a,b, Extended Data Figure 9a–c), together with increased infiltrating IFNγ producing Th1 polarized T cells (Extended Data Fig 9d–i). The increased EAE susceptibility in heterozygous mice is important as only partial loss of C9orf72 expression is observed in repeat expansion carrier tissues, and indicates that incorporation of an environmental stressor is necessary as heterozygous DCs did not show baseline differences in immune cell activation markers. This supports a model whereby chronic STING activation in DCs promotes activation of Th1 polarized T cells, which infiltrate the nervous system during EAE and drive the enhanced inflammatory response. This finding is of interest given the recent report that *C9orf72* repeat expansion mutations were overrepresented in patients with the rare combination of ALS and multiple sclerosis, for which EAE is used as a model[26]. Importantly the chronic STING activation in myeloid cells and adaptive immune cell activation seen in *C9orf72*$^{-/-}$ mice is distinct from acute STING activation during EAE, which mitigatews severity by directly promoting T regulatory responses and suppressing Th1 responses[27].

Interestingly studies have also suggested altered frequency of various cancers in patients with ALS[28]. Dendritic cells play a central role in maintaining the tone of the immune system, with a propensity toward autoimmunity also associated with enhanced anti-tumor immunity[10,11]. We therefore examined an animal model of anti-tumor immunity in *C9orf72*$^{-/-}$ mice by measuring tumor burden after intravenous injection of mouse B16

melanoma cells. We observed a *C9orf72* gene dose dependent decrease in B16 melanoma tumor burden in the lungs, with mice lacking either one or both copies of *C9orf72* being more resistant than wildtype mice (Fig 3c–e), accompanied by increased activated T cells in the lung and the spleen after B16 inoculation (Extended Data Fig 10). These data are consistent with a prior study showing that STING mediated sensing of tumor DNA is critical for priming anti-tumor CD8 effector T cells[29]. Our data similarly suggest that enhanced STING/type I IFN responses to tumor derived DNA in *C9orf72*$^{-/-}$ DCs more effectively drive cytotoxic anti-tumor T cells. In summary, these findings indicate that the altered immunophenotype observed in *C9orf72*$^{-/-}$ mice from loss of even one copy of *C9orf72* leads to enhanced susceptibility to autoimmune disease, and increased anti-tumor immunity.

To assess whether a similar altered immunophenotype exists in myeloid cells from *C9orf72* repeat expansion carriers, we examined blood monocyte derived macrophages (MDMs) from normal controls, sporadic ALS patients, and C9-ALS patients using RNA-seq. Gene set enrichment analysis (GSEA) showed marked upregulation of pathways related to IFN-α/β signaling in C9-ALS MDMs vs. sporadic ALS MDMs, overlapping nearly identically to upregulated pathways seen in immune cells from *C9orf72*$^{-/-}$ mice (Fig. 4a–c; see Fig. 1g). We looked to confirm these findings in a larger validation set, examining whole blood RNA-seq data from patients with either sporadic ALS (n=259) or C9-ALS (n=20). We confirmed the lower expression of *C9orf72* in C9-ALS carriers previously reported (Fig. 4d, $p=3.37\times10^{-7}$, Mann-Whitney U test), and again observed a significant upregulation of type I IFN signaling on GSEA in C9-ALS vs. sALS patients (Fig 4e). To assess whether this genotype driven inflammatory signature was present in nervous tissue, we analyzed transcriptome data from a previously published RNA-seq dataset of ALS patients[30]. We examined cerebellar tissue to avoid the variability of inflammation observed in actively degenerating regions such as frontal cortex. We again observed decreased levels of *C9orf72* expression, and upregulation of the type I interferon response by GSEA in the cerebellum of C9-ALS patients vs. sporadic ALS patients (Fig 4f). To determine if this elevated type I IFN signature could be from microglial cells, we examined IFNβ production from isolated mouse microglia after cGAMP stimulation, and observed a similar hyperactive response to STING activation comparable to peripheral macrophages in *C9orf72*$^{-/-}$ mice (Fig 4g). Finally, to determine if the elevated type I IFN signaling observed in C9-ALS patient myeloid cells is driven by STING, we treated patient PBMCs or MDMs with a STING inhibitor. We observed in mixed PBMCs that the STING inhibitor H151 did not alter basal ISG expression in sporadic ALS patients, but consistently suppressed ISG expression in C9-ALS PBMCs (Fig 4h). We observed a similar ISG suppression across the broader signature using RNA-seq from H151 treated C9-ALS patient MDMs (Fig 4i). These findings strongly support that C9-ALS/FTD carriers have a genetically determined immunophenotype characterized by hyperactive type I interferon signaling that can be detected in either blood or brain tissues across multiple independent datasets, that is driven at least partly by STING activation.

In summary, *C9orf72* in myeloid cells including DCs is essential for maintaining immune homeostasis, with loss of C9orf72 promoting hyperactive type I interferon production, and adaptive immune activation with enhanced autoimmunity and anti-tumor immunity. The hyperactive type I IFN response in *C9orf72*$^{-/-}$ DCs was mitigated by blocking STING, which was also recently implicated in inflammation in Parkinson's disease models[31]. Of

note, DC specific knockout of *Tbk1*, another ALS/FTD disease gene involved in the cGAS-STING pathway, manifested a similar immunophenotype with mice developing systemic IFN driven inflammation, increased propensity for autoimmune disease and cancer resistance, supporting a convergence of C9orf72 and TBK1 signaling pathways in ALS/FTD[32]. However the paradoxical nature of elevated type I IFN signaling in TBK1 deficient DCs suggests that TBK1 does not solely act as a downstream effector of STING[32]. A key finding of our study is that the increased type I IFN signature was present in C9-ALS carrier myeloid cells, whole blood and brain tissue, serving as a potential biomarker of C9orf72 function in these patients. We hypothesize that decreased *C9orf72* expression in C9-ALS/FTD carriers promotes this enhanced IFN production, altering their response to environmental factors such as trauma or infection, and may influence subsequent development of ALS, FTD and/or autoimmunity. Additionally, the loss of function effects on microglia and peripheral dendritic cells may exacerbate the toxic gain of function manifestations of the C9orf72 expansion in neurons or other cell types.

## Methods

### Mice.

All mice were housed in pathogen-free facilities under 12-h light dark cycles with access to food and water ad libitum. Temperature was set 74°F +/− 2° with humidity 30–70%. *C9orf72*$^{-/-}$ mice were as previously published[7] and wildtype mice were purchased from Jackson Laboratories. *C9orf72*$^{fl/fl}$ mice were provided by the Pasterkamp lab[12] and were crossed with Cx3cr1$^{Cre}$ (B6J.B6N(Cg)-*Cx3cr1*$^{tm1.1(cre)Jung}$/J) and Lyz2$^{Cre}$ (B6.129P2-*Lyz2*$^{tm1(cre)Ifo}$/J) purchased from Jackson Laboratories to obtain Cx3cr1$^{Cre}$;C9orf72$^{fl/fl}$ and Lyz2$^{Cre}$;C9orf72$^{fl/fl}$ mice. The STING *golden-ticket* (STING*gt/gt*) mouse was obtained from Jackson Laboratories (C57BL/6J- Tmem173gt/J). C9orf72$^{-/-}$ mice were crossed with STING*gt/gt* to obtain *C9orf72*$^{-/-}$;STING$^{gt/gt}$ mice. All mice have the nuclear background of C57BL/6J. Mice were sex- and age-matched. For all experiments mice were grouped according to genotype. For EAE and B16 melanoma models genotypes were randomly separated into experimental groups. Researchers were blinded when scoring EAE, counting tumor burden in B16 melanoma model. Husbandry and behavioral tests were conducted in accordance with the protocols described by the National Institutes of Health's Guide for the Care and Use of Animals and were approved by Cedars-Sinai Institutional Animal Care and Use Committees (IACUC #8161).

### Flow cytometry and FACS sorting.

Single-cell suspensions were removed of red blood cells (RBC lysis buffer, Sigma). Cells were incubated in Fc block (anti-CD16/anti-CD32) prior to staining to prevent nonspecific antibody binding. An LSRFortessa (BD Bioscience) was used for flow cytometry and data was analyzed with BDFacs Diva and FlowJo. Dendritic cells (CD11c+, PDCA1+, CD8+, CD11b+), B cells (CD19+), CD4 T cells (CD3+CD4+), CD8 T cells (CD3+CD8+) and CD11b+ cells were purified from splenocytes by fluorescence-activated cell sorting (FACS) using a FACSAria II cell sorter (BD Biosciences). Gating strategies can be found in Supplemental Information Guide.

### Antibodies.

All antibodies for flow cytometry were 1:200 dilution. CD4 PE: BioLegend: 100408, BD Biosciences: 563106, CD8α BioLegend:100722, CD44 BD Biosciences:103011, I-Ab (MHC II) BioLegend:116416, CD40 BD Biosciences: 561846, CD80 BD Biosciences: 565820, CD86 BioLegend:105008, CD62L BD Bioscience:560507, CD11c BioLegend:117310, CD11b: BioLegend: 101263, 101206, PDCA1 BioLegend:127008, CD3 BioLegend:100311, TNFα Biolegend:506306, IFNγ Biolegend:505805, IL17 Biolegend:506917, Foxp3 eBioscience,17–5773-80B, CD19 BioLegend:115508, LEAF Purified anti-mouse CD3 Biolegend:100314, LEAF Purified anti-mouse CD28 BioLegend:102112, Propidium iodide solution BioLegend:79997, Fc block 2.4G2 cell supernatant ATCC: HB-197; RRID: AB_2103740.

### T cell activation and cytokine production.

Single-cell suspension of total splenocytes were removed of red blood cells (RBC lysis buffer, Sigma). CD4 T cells were isolated using EasySep™ Mouse Isolation Kit (StemCell Technologies). For stimulated wells, 96-well plates were pre-coated with 2ng/μl of anti-CD3 overnight in 4° C. Wells were washed with PBS 3x and $1\times10^6$ CD4 T cells were plated in 100μl per well along with 2ng/μl anti-CD28. Supernatants were collected after 72 hours and ELISAs were run for IFNγ, IL-2, IL-4, and IL-17 (BioLegend).

### Treg and intracellular cytokine staining.

**Tregs:** Cells were collected and washed with 1ml of staining buffer (0.045g Sodium Azide, 5% FBS in PBS) and resuspended in Fc Block for 20 minutes followed by incubation with surface staining antibodies at 4°C. Intracellular staining of Foxp3 was done using Foxp3/Transcription factor staining buffer set (eBioscience Cat#00–5523). In brief, fixation/permeabilization buffer was added and cells were incubated for 60 minutes room temperature in the dark. Cells were washed with 1x permeabilization buffer and intracellular antibodies were added overnight. The following day cells were fixed and analyzed via flow cytometry with LSRFortessa.

**TNFα staining:** total splenocytes were stimulated with LPS overnight. PLUG was added to the wells for 3 hours. Cells were collected and resuspended in Fc block for 10 minutes followed by incubation with surface staining antibodies at 4°C for 15 minutes. Cells were washed and resuspended in cytofix/cytoperm (BD Biosciences, Cat#554714) overnight. The next day cells were resuspended in rat serum for 15 minutes at room temperature and intracellular antibodies were added for another 15 minutes. Cells were washed, fixed and analyzed via flow cytometry with LSRFortessa.

### Generation and stimulation of BMDM.

Bone marrow cells were isolated from femurs and tibias of mice and cultured for 7 days in RPMI medium including 10% FBS and 1% Penicillin-Streptomycin-Glutamine with 50ng/ml hM-CSF (Peprotech). Cells were plated 350,000/700μl and stimulated with LPS (100ng/ml), Poly I:C (10ng/ml), CpG (1μg/ml) or cGAMP (5μg/ml unless otherwise stated). STING antagonist H151 (Cayman chemicals) was added 30 minutes before stimulation.

### Peripheral blood mononuclear cells and monocyte Derived Macrophage (MDM) differentiation.

Peripheral blood mononuclear cells (PBMCs) were isolated from human blood samples collected in BD Vacutainer CPT tubes and centrifuged at 1600 RCF for 20 minutes. The plasma and PBMCs were collected and centrifugation (300 xg, 10 minutes) to isolate the PBMCs. PBMCs were plated overnight and STING antagonist H151 (Cayman chemicals) was added for 6 hours before RNA was collected. For monocyte derived macrophages (MDMs), the CD14+ cells were isolated from the PBMCs using the magnetic CD14 beads from Miltenyi biotec according to the manufacturer's instructions, then cultured in IMDM + 10% FBS + hMCSF (50ng/ml) for 7 days, and collected for RNA. For STING inhibitor experiments, 1μM STING antagonist H151 (Cayman chemicals) was added on day 7 for 6 hours before RNA was collected.

### Isolation and stimulation of microglia.

**Microglia isolation:** Wildtype and C9 null mice were perfused with PBS/Heparin, their brains isolated and dissociated using the Neural dissociation kit (Miltenyi Biotech) and GentleMACS dissociator (NTDK Brain setting). The lysate was collected and passed through a 70μm strainer to obtain a single cell suspension. Next, myelin was removed from the cells by incubating with magnetic myelin beads (Myelin Removal Beads II, human, mouse, rat, Miltenyi Biotech) using the AutoMACs. Cells were then incubated with CD11b+ magnetic beads (CD11b (Microglia) MicroBeads, human and mouse, Miltenyi Biotech) and sorted using the AutoMACs. The CD11b+ cells were counted, plated (200K cells/well) and cultured in Microglia complete media containing DMEM/F-12, GlutaMAX™with HEPES (Invitrogen), 10% fetal bovine serum, 100μg/ml Penicillin/ Streptomycin/0.25μg/ml fungizone, with 10 ng/ml of the following growth factors: Recombinant mouse M-CSF, Recombinant mouse GM-CSF (R&D systems) and 50ng/ml TGF-β1 (Miltenyi Biotech) for 6 days before stimulation.

**Microglia stimulation:** 6 days post culturing, microglia were stimulated with 10ug/ml cGAMP for 8 hrs. Post stimulation, cells were lysed in lysis buffer and RNA isolated using Qiagen MIcro RNA isolation kit. RNA quality was determined using Nanodrop and 200ng of RNA was used to make cDNA.

### Isolation of splenic immune cells.

Splenic immune cells were isolated by mechanical disruption of spleens in PBS with 0.4% EDTA and 0.5% FBS. The cell suspension was spun down at 1600rpm for 4 minutes and resuspended in red blood cell lysis buffer (Sigma-Aldrich) for 2.5 minutes. Cells were then washed, resuspended in Fc block for 10 minutes followed by incubation with anti-CD11c and anti-PDCA1 (DCs), anti-CD3 and anti-CD4/CD8 (T cells), anti-CD11b (myeloid cells) and anti-CD19 (B cells) at 4C for 15 minutes, washed and purified by flow cytometry using FACSAria II flow cytometer (BD).

### RNA isolation and qRT-PCR and Western blot analysis.

RNA was isolated using PureLink RNA Mini kit (Invitrogen). RNA was reverse-transcribed to cDNA with oligo(dT) with the Promega Reverse Transcriptase System and analyzed using SYBR Green Master Mix (Applied Biosystems). Mouse primers: IFNβ (Forward – 5'-AGCTCCAAGAAAGGACGAACAT-3'and Reverse- 5'-GCCCTGTAGGTGAGGTTGATCT-3'), Mx1 (Forward- 5'-AAACCTGATCCGACTTCACTTCC-3' and Reverse-TGATCGTCTTCAAGGTTTCCTTGT-3'), Cxcl10 (Forward- 5'-CCAAGTGCTGCCGTCATTTTC-3' and Reverse- 5'-GGCTCGCAGGGATGATTTCAA-3'). Expression was normalized to mouse 18S (Forward-5'-GATGGTAGTCGCCGTGCC-3' and Reverse- 5'-GCCTGCTGCCTTCCTTGG-3'). Trem 2 (Forward – 5'-GACCTCTCCACCAGTTTCTCC-3' and Reverse- 5'-TACATGACACCCTCAAGGACTG-3'), IL10 (Forward-5'CCAGAGCCACATGCTCCTAGA'3 and Reverse 5'-GGTCCTTTGTTTGAAAGAAAGTCTTC-3'). Expression was normalized to mouse Actin (Forward- 5'AGGTATCCTGACCCTGAAG-3' and Reverse- 5'-GCTCATTGTAGAAGGTGTGG-3'). Human primers: Mx1 (Forward- 5' GGTGGTCCCCAGTAATGTGG-3' and Reverse- 5' CGTCAAGATTCCGATGGTCCT-3'), STAT1 (Forward- 5' TGTATGCCATCCTCGAGAGC-3' and Reverse- 5' AGACATCCTGCCACCTTGTG-3'), IFI44L (Forward-5' TTGTGTGACACTATGGGGCTA-3' and Reverse- 5' GAATGCTCAGGTGTAATTGGTTT-3'), ISG15 (Forward- 5' GAGGCAGCGAACTCATCTTT-3' and Reverse- 5' AGCATCTTCACCGTCAGGTC-3') and IFI27 (Forward- 5' GTGGCCAAAGTGGTCAGG-3' and Reverse- 5' CCAATCACAACTGTAGCAATCC-3'). Expression was normalized to RPL13A (Forward-5' CCTGGAGGAGAAGAGGAAAGAGA-3' and Reverse- 5' TTGAGGACCTCTGTGTATTTGTCAA-3') or B2M (Forward- 5' TGCTGTCTCCATGTTTGATGTATCT-3' and Reverse- 5' TCTCTGCTCCCCACCTCTAAGT-3'). Data shown are technical replicates with each experiment being repeated in the laboratory with biological replicates 3–4 times.

For western blots, equal number of cells were lysed in 1x NuPAGE sample buffer (2.5% BME), transferred to nitrocellulose membranes, and probed with LC3 (Novus Biologicals #NB100–2220, 1:000), STING (Cell Signaling Technology #13647, 1:1000), phospo-STING Ser365 (Cell Signaling Technology #72971, 1:500), Tubulin (Sigma-Aldrich #T6074, 1:1000), and GAPDH (Sigma-Aldrich #G8795, 1:5000) primary antibodies. The proteins were detected using the LI-COR system, blocking buffer, and secondary antibodies (1:15000).

### RNA-seq of mouse splenic dendritic cells.

Splenic DC RNA quality was assessed via bioanalyzer (Agilent) and quantified via Qubit fluorometric quantification (Thermo Fisher). RNA-seq libraries were generated using 200ng total RNA as input for the TruSeq Stranded mRNA Library Prep kit (Illumina) according to the manufacturer's protocol, and samples were indexed using TruSeq RNA Single Indexes (Illumina). Library preps were analyzed via bioanalyzer (Agilent) and quantified via Qubit

fluorometric quantification (Thermo Fisher). Quantified libraries were normalized, pooled, and sequenced on a NextSeq 500 sequencer (Illumina) using the single-end 75 nucleotide setting. Raw sequencing reads were demultiplexed, and FASTQ files were aligned to the mouse genome (mm10) via Tophat v2.1.1 and Bowtie v2.3.2. BAM files were indexed with Samtools v1.6 and annotated using Partek software v7.17.0918 to generate RPKM values for each gene.

## RNA-seq library preparation and Gene Set Enrichment Analysis of mouse B cells, CD4+ T cells, CD8+ T cells and CD11b+ cells

RNA quality was assessed via bioanalyzer (Agilent) and quantified via Qubit fluorometric quantification (Thermo Fisher). RNA-seq libraries were generated using 200ng total RNA as input for the TruSeq Stranded mRNA Library Prep kit (Illumina) according to the manufacturer's protocol, and samples were indexed using TruSeq RNA Single Indexes (Illumina). Library preps were analyzed via bioanalyzer (Agilent) and quantified via Qubit fluorometric quantification (Thermo Fisher). Quantified libraries were normalized, pooled, and sequenced on a NextSeq 500 sequencer (Illumina) using the single-end 75 nucleotide setting. Raw sequencing reads were demultiplexed, and FASTQ files were used to generate estimated transcript counts against the mouse transcriptome (mm10) via Salmon v0.8.2. TPM values summed to the gene level were generated using the R Bioconductor package DEseq2. Median TPM values were calculated within each cell type. Genes with a median TPM value less than 0.5 within each cell type were discarded. The union of the remaining genes from each cell type were combined, and the signal-to-noise metric (difference in mean expression divided by the sum of standard deviations, $(\mu A - \mu B)/(\sigma A + \sigma B)$) was calculated for each of these remaining 12,174 genes when comparing between each genotype group within each cell type. These gene values were ranked from highest to lowest, indicating which genes were most upregulated and downregulated with the least variation. These sorted lists of genes were used as inputs for Gene Set Enrichment Analysis (GSEA), using 1000 permutations of the gene sets. A false discovery rate P-value less than 0.05 was accepted as significant.

### RNA-seq of monocyte derived macrophages.

RNA quality was assessed via bioanalyzer (Agilent) and quantified via Qubit fluorometric quantification (Thermo Fisher). RNA-seq libraries were generated using an average of ~150ng total RNA as input for the TruSeq Stranded mRNA Library Prep kit (Illumina) according to the manufacturer's protocol, and samples were indexed using TruSeq RNA Single Indexes (Illumina). Library preps were analyzed via bioanalyzer (Agilent) and quantified via Qubit fluorometric quantification (Thermo Fisher). Quantified libraries were normalized, pooled, and sequenced on a NextSeq 500 sequencer (Illumina) using the single-end 75 nucleotide setting. Raw sequencing reads were demultiplexed, and FASTQ files were aligned to the human genome (hg38) via Tophat v2.1.1 and Bowtie v2.3.2. BAM files were indexed with Samtools v1.6 and annotated using Partek software v7.17.0918 to generate RPKM values for each gene. RPKM values were log2 transformed after adding a pseudocount of 1. Genes with a median log2 transformed RPKM value less than 0.5 were discarded. Signal to noise ratios of the remaining genes were calculated for each group

comparison, and the sorted list of these genes was used as the input for GSEA using 1000 permutations of the gene sets. A false discovery rate P-value of less than 0.05 was accepted as significant.

### RNA-seq analysis of human whole-blood data.

RNA-seq libraries were generated using total RNA as input for the TruSeq mRNA Library Prep kit (Illumina) according to the manufacturer's protocol, and samples were indexed using TruSeq RNA Single Indexes (Illumina). Samples were pooled and sequenced on a NovaSeq 6000 sequencer (Illumina) using the paired-end 151nt setting. Due to read 2 sequencing errors in a subset of the samples, all samples were aligned as single-ended datasets using read 1 only. RNA-seq reads were aligned to hg19 using STAR (v.2.5.3). Expression was quantified using RSEM (v1.3.0) with the following flags: --fragment-length-max 1000, --no-bam-output, --estimate-rspd. Given the heterogeneity in expression signatures from whole blood expression data, expression data were first normalized using PEER v1.3 (Probabilistic Estimation of Expression Residuals, PMID #22343431), setting 35 hidden determinants (K=35) and allowing up to 1000 iterations. In addition, the following known co-variates were included: sex, collection subsite, age at onset, years to diagnosis, ALS functional rating scale, and sample ancestry estimated by PCA, with categorical variables binarized before inclusion. After filtering against non-expressed genes (TPM<1 for all individuals), differential expression analysis was performed using a trans-QTL approach using the R/qtl package (version 1.44–9) on PEER residuals using the C9orf72 locus repeat expansion genotype against the entire transcriptome (see step 13 in PMID 22343431 for additional details). GSEA analysis was performed against the GO gene sets category in MSigDB, and enrichments were visualized using the Enrichment Map plug-in (v3.2.0, PMID 21085593) in Cytoscape (v.3.7.1).

### RNA-seq analysis of human cerebellum.

For the human GSEA, the raw count table was obtained from (Prudencio et al, 2015)[30] series GSE67196 for the control, sporadic, and C9orf72 repeat carrier patient frontal cortex and cerebellum samples. RPKM values were derived for these samples using the edgR package in R Bioconductor. Total raw counts in each sample were used as the library size, and the transcript lengths for each HGNC identifier were obtained from Ensembl BioMart. Calculating the median RPKM values for each gene and discarding all genes with a median value below 1 filtered for 11912 genes used in GSEA. The signal-to-noise metric (difference in mean expression divided by the sum of standard deviations, $(\mu A - \mu B)/(\sigma A + \sigma B)$) was calculated for each gene when comparing frontal cortices or cerebella between sporadic or C9orf72 ALS cases to control groups. These gene values were ranked from highest to lowest, indicating which genes are most up-regulated and downregulated with the least variation. GSEA was performed on these ranked gene lists with 1000 permutations of the gene sets and a false discovery rate P-value of less than 0.05 was accepted as significant.

### Gene Set Enrichment Analysis.

RPKM or FPKM values were log2 transformed after adding a pseudocount of 1. Genes with a median log2 transformed R/FPKM value less than 0.5 were discarded. Signal to noise

ratios of the remaining genes were calculated for each group comparison, and the sorted list of these genes was used as the input for GSEA.

### Induction and assessment of EAE.

Disease induction was as described by Hooke labs and lot #1004 and lot #1006 were used in this study. In brief, females aged 10–13 weeks were immunized s.c with $MOG_{35–55}$ peptide mixed with CFA on day 0. Pertussis toxin was administered at 120ng/dose i.p on days 0 and 1. Mice were examined daily starting at day 7 and scored for disease severity on the scale: 0, no clinical score; 0.5, tip of the tail paralysis; 1, total tail paralysis; 1.5, limp tail and hind leg inhibition; 2, limp tail and weakness of hind legs; 2.5, limp tail and dragging of hind legs; 3, limp tail and complete paralysis of hind legs; 3.5, limp tails, paralysis of hind legs and unable to right themselves; 4, limp tails, complete hind legs and partial front leg paralysis; 4.5, no movement around cage; 5, euthanasia. After onset of disease, mice are singly housed and food and water are provided on the cage floor. For time course experiment, mice were taken down at onset (day 11) and peak (day 15) and spleens and brain were collected. Myelin was removed from the brain (Miltenyi Biotec Cat. # 130–096-733). Single cell suspension was stained intracellularly with IFNγ and IL-17.

### Cells and tumor models.

The mouse melanoma cell line B16F10 was obtained from ATCC® (CRL-6475) and was maintained in Dulbecco's Modified Eagle's Medium (DMEM) supplemented with 10% fetal bovine serum (FBS), penicillin (100 U/ml), and streptomycin (100 μg/ml). For lung metastatic models, B16 ($2\times10^5$) cells were injected via tail vein and were enumerated visually facilitated by the use of a magnifying glass and a lamp or by extracted melanin determined by spectrophotometry. Tumour measurements/volumes did not exceed what is permitted by Cedars-Sinai IACUC. To extract melanin, the entire left lobe was placed into a homogenizer and was digested in 300 μL of PBS. The sample was then centrifuged for 10 minutes at max speed and the supernatant was removed. The samples were then processed in 1 mL of lysis buffer contained 1M tris-Hcl, 10%SDS, 0.5 M EDTA, 10 μg/mL Proteinase K, and water in a shaker at 56°C until completely dissolved. This process can take up to 48 hours and was aided by the addition of additional proteinase K and processing through an 18 gauge needle. Once the melanin was dissolved, samples were centrifuged for 10 minutes at max speed and the supernatant was discarded so that a black pellet remained at the bottom. 200 μL of 2N NaOH was added and the sample was placed in a shaker at 95°C overnight or until completely dissolved. Once the melanin was dissolved, 100 μL of 2 chloroform:1 methanol were added and the sample was mixed well before being centrifuged for 10 minutes at max speed. 100 μL of the top layer was read on a SpectraMax spectrophotometer: OD405-OD570. Resulting values were analyzed directly. For T cell activation studies, mice were sacrified 14 days after i.v injection and lungs and spleens were collected. The lung was selected and the tissue was manually digested in a lysis buffer containing HBSS, collagenase, and DNAseI with two 10 minute incubations at 37°C. Samples were centrifuged for 5 min at 3000 RPM and the red blood cells were lysed using 1X RBC lysis buffer (eBioscience). The cells were then washed and stained with an Fc blocker to prevent any non-specific binding. Single cells from digested lung were stained with anti-CD3, anti-CD4, anti-CD8 and anti-CD44 and were washed and fixed. Spleens were collected as

described previously, stained for anti-CD3, anti-CD4, anti-CD8 and anti-CD44, washed, fixed and analyzed via flow cytometry with LSRFortessa. Age matched T cells from naïve mice were used to compare the activation state of T cells with and without B16 inoculation.

### Statistical Analyses.

Statistical tests used are indicated in figure legends. All data are shown as mean ± SEM, and all analyses were conducted using Prism software (Graphpad).

## Extended Data

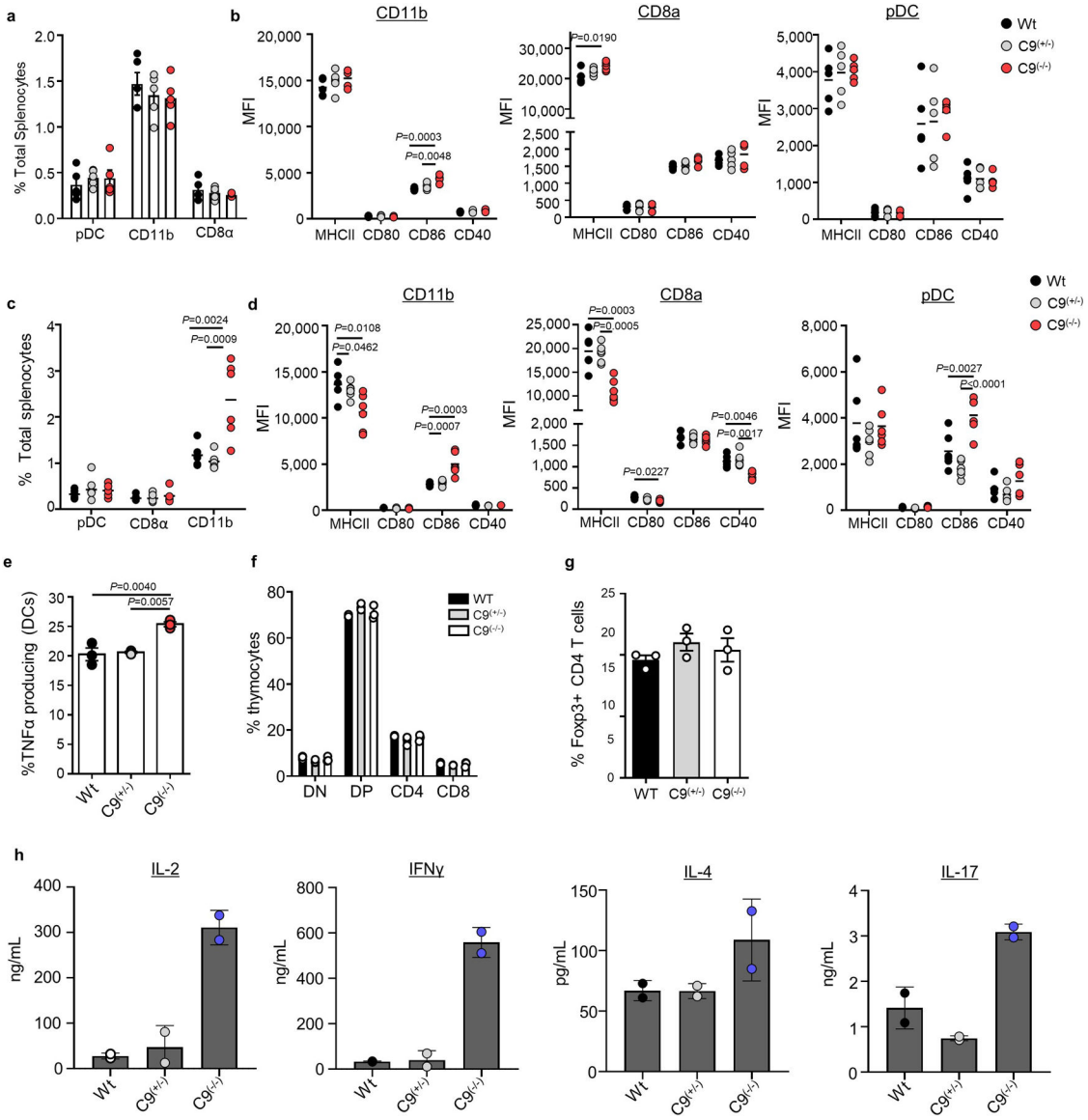


**Extended Data Fig. 1|. Dendritic cells and T cells develop normally in *C9orf72*$^{-/-}$ mice, but show markers of immune activation and inflammatory cytokine production from a young age.**

**a.** Percentage of dendritic cell (DC) populations from total splenocytes of 8-week old mice (n=5). **b.** MFI measured via flow cytometry for MHCII and co-stimulatory molecules

(CD80, CD86, and CD40) of three splenic DC populations (CD11b, CD8a, and pDC) from 8-week old mice (n=5). **c.** Percentage of DC populations from total splenocytes of 8-month old mice (n=6). **d.** MFI measured via flow cytometry for MHCII and co-stimulatory molecules of splenic DC populations of 8-month old mice (n=6). **e.** Intracellular TNFα staining of splenic DCs from 10-week old mice after LPS (100ng/ml) stimulation (n=3). **f.** Quantification of double negative (DN), double positive (DP) and single positive CD4 and CD8 T cell populations in thymus of 8-week old mice (n=3). **g.** Percentage of Foxp3+ CD4 T cells in the spleen of 8 week old mice (n=3) showing no change in T regulatory cell populations. **h.** ELISA of supernatants collected from isolated CD4 T cells of 6-month old mice from spleen after anti-CD3/anti-CD28 treatment for 72 hours, graphs duplicate measurements from two independent experiments. **a-h.** One-way ANOVA. **e,h,i.** Data are presented as mean values +/− SEM. **h.** Data are presented as mean values +/− SD.

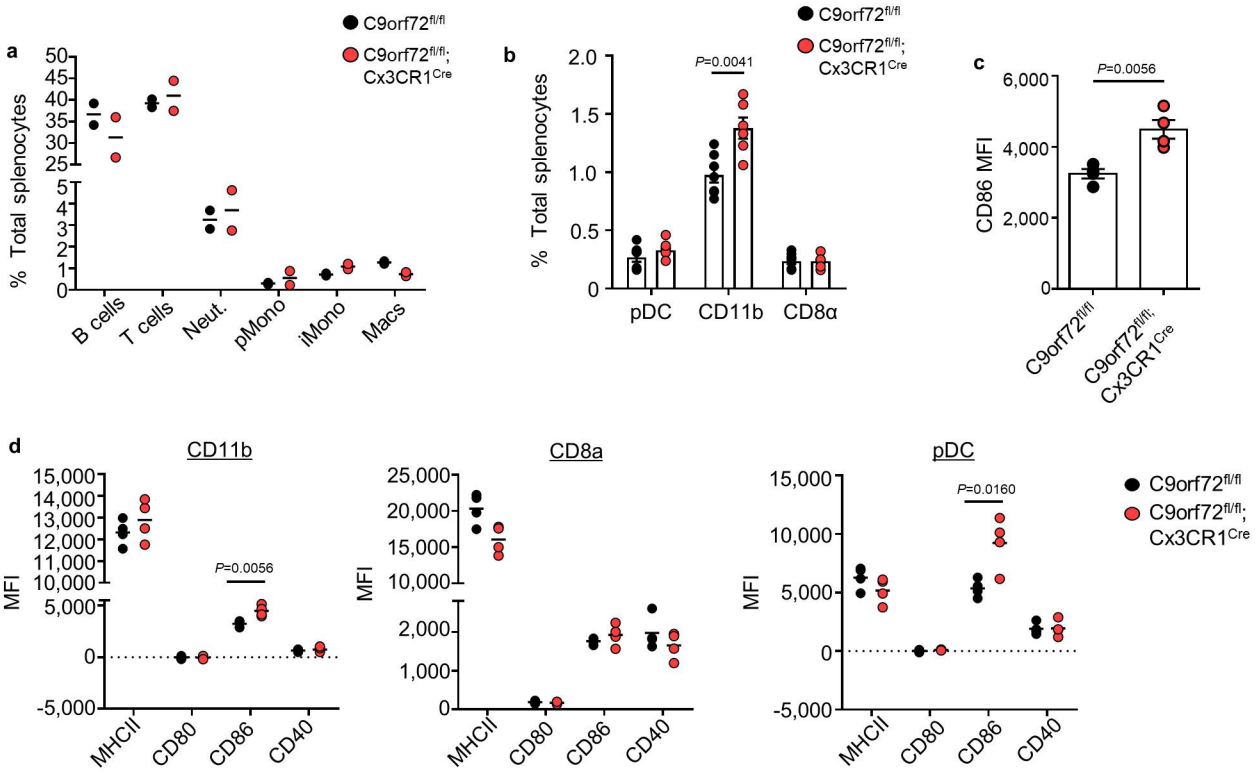


**Extended Data Fig. 2|. Profiling of splenocytes from myeloid specific deletion of *C9orf72* via Cx3cr1-Cre.**

**a.** Proportion of immune cell populations in 12-month old *C9orf72*$^{fl/fl}$:Cx3cr1$^{Cre}$ mice. **b.** Proportion of splenic DC populations in 5-month old *C9orf72*$^{fl/fl}$:Cx3cr1$^{Cre}$ mice (n=7). **c.** *C9orf72*$^{fl/fl}$:Cx3cr1$^{Cre}$ CD11b splenic DCs have increased MFI of CD86 in 5-month old mice (n=4). **d.** MFI of splenic DC MHCII and co-stimulatory molecules in 5-month old *C9orf72*$^{fl/fl}$:Cx3cr1$^{Cre}$ mice (n=7). Unpaired, two-tailed Students t-test. **b,c.** Data are presented as mean values +/− SEM.

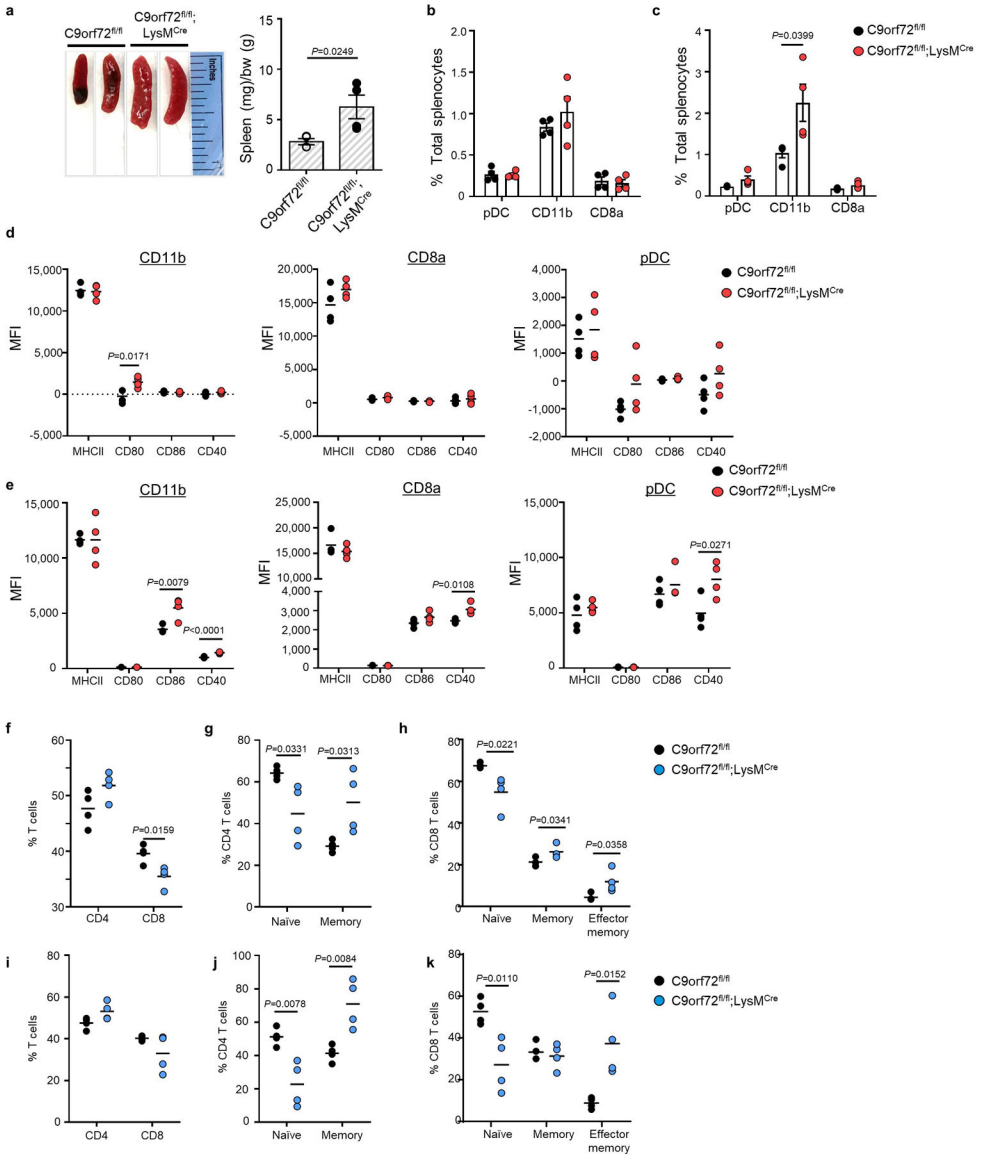


**Extended Data Fig. 3|. Immune profiling of *C9orf72*$^{fl/fl}$:LysM$^{Cre}$ mice.**

**a.** Gross images of splenomegaly in *C9orf72*$^{fl/fl}$:LysM$^{Cre}$ (left) Spleen weights of *C9orf72*$^{fl/fl}$:LysM$^{Cre}$ (mg) normalized to body weight (g) at 5 months (right) (n=4). **b.** Proportion of splenic DC populations in 5-month old *C9orf72*$^{fl/fl}$:LysM$^{Cre}$ mice (n=4) **c.** Proportion of splenic DC populations in 12-month old *C9orf72*$^{fl/fl}$:LysM$^{Cre}$ mice (n=4). **d.** MFI of splenic DC MHCII and co-stimulatory molecules in 5-month old *C9orf72*$^{fl/fl}$:LysM$^{Cre}$ mice (n=4). **e.** MFI measured via flow cytometry for MHCII and co-stimulatory molecules of splenic DC populations of 12-month old *C9orf72*$^{fl/fl}$:LysM$^{Cre}$ mice (n=4). **f.** Percentage of CD4 and CD8 T cells in splenocytes. **g.** CD4 T cell and **h.** CD8 T cell activation states in 5-month of *C9orf72*$^{fl/fl}$:LysM$^{Cre}$ mice. **i.** Percentage of CD4 and CD8 T cells in splenocytes in 12-month old mice. **j.** CD4 T cell and **k.** CD8 T cell activation states in 12-month old *C9orf72*$^{fl/fl}$:LysM$^{Cre}$ mice (n=4). Unpaired, two-tailed Students t-test. **a-c.** Data are presented as mean values +/− SEM.

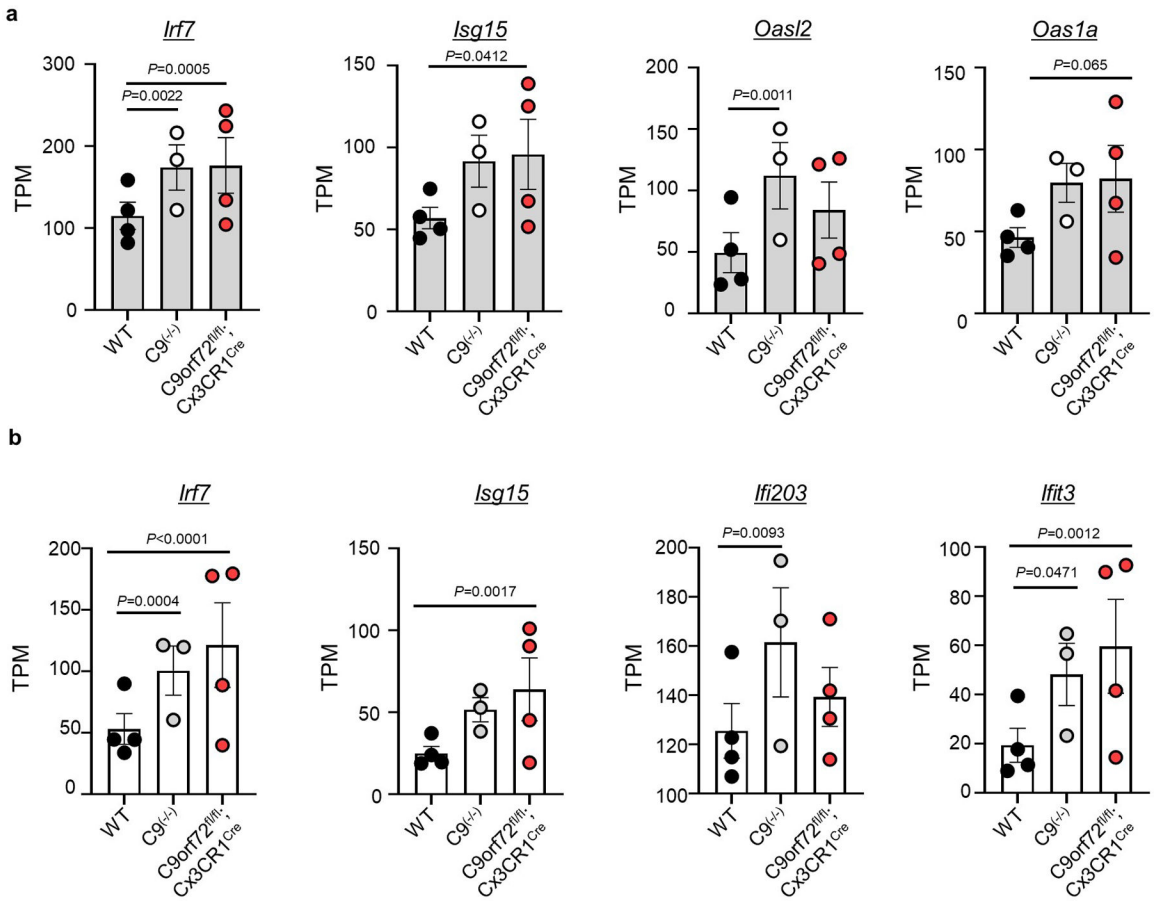


**Extended Data Fig. 4|. RNA-seq values for type I interferon stimulated genes in different immune populations of total body versus myeloid cell specific deletion of *C9orf72*.**

**a.** RNA-sequencing of CD11b cells (**a**) and B cells (**b**) from wildtype (WT; n=4), total knockout ($C9^{(-/-)}$;n=3) and $C9orf72^{fl/fl}$:$Cx3cr1^{Cre}$ (n=4) mice, similar to that observed in dendritic cells of the total body nulls (Fig 2), showing activation of ISGs. T cells from the same data set are shown in main Fig 1. Two-way ANOVA. Data are presented as mean values +/− SEM.

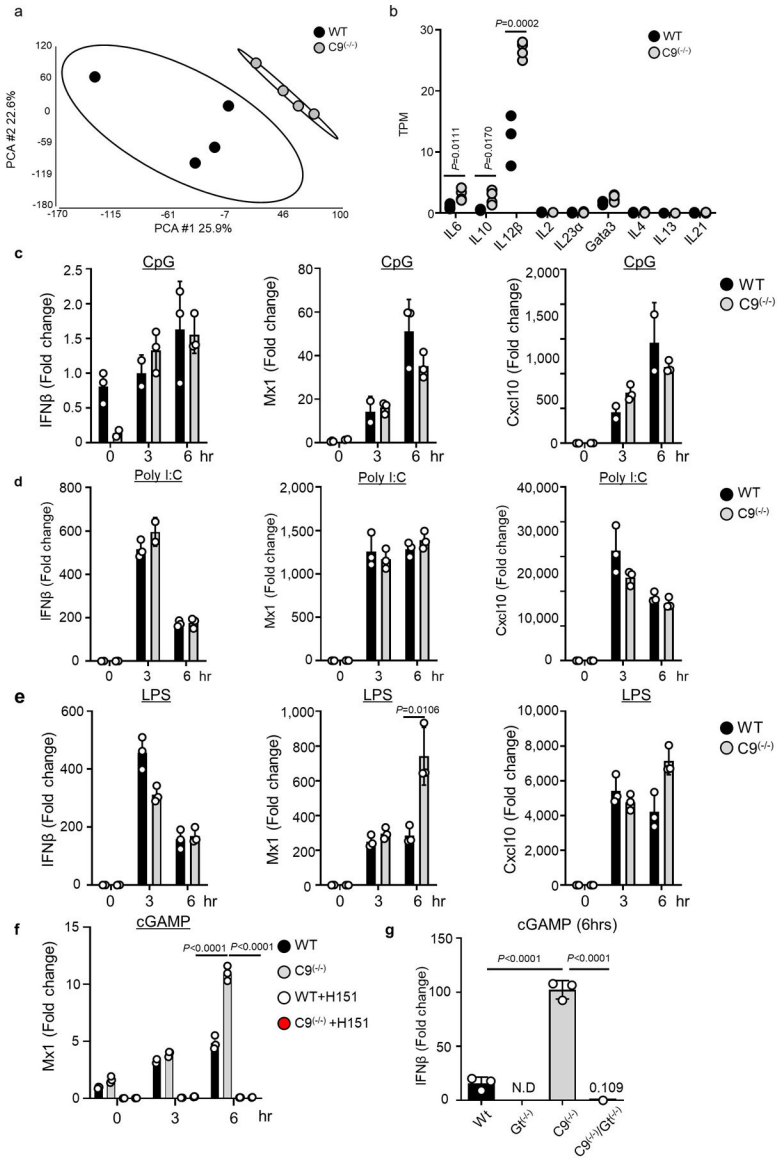


**Extended Data Fig. 5|. RNA-seq of *C9orf72* deficient DCs, ISG responses in BMDM to TLR agonists, and amelioration of type I IFN responses by deleting STING.**

**a.** PCA plot of RNA sequencing of freshly isolated splenic classical DCs from 10-week old mice (n=4). **b.** TPM of indicated cytokines and inflammatory genes (WT n=4, $C9^{(-/-)}$ n=4 biologically independent samples). **c-e.** qRT-PCR of Ifnβ, Mx1 and Cxcl10 in WT and $C9^{(-/-)}$ BMDMs after stimulation of **c.** CpG, **d.** Poly IC and **e.** LPS (representative of 3 experiments) **f.** STING antagonist H151 blocks the hyperactive ISG response to cGAMP stimulation (representative of 3 experiments). **g.** qRT-PCR of IFNβ in total BMDMs of WT, $Gt^{(-/-)}$, $C9^{(-/-)}$ and $C9^{(-/-)}$:$Gt^{(-/-)}$ mice after cGAMP stimulation. Representative of 3 independent experiments. **b-e.** Unpaired, two-tailed t-test. **f,g.** One-way ANOVA. **b.** Data are presented as mean values +/− SEM. **c-g.** Data are presented as mean values +/− SD.

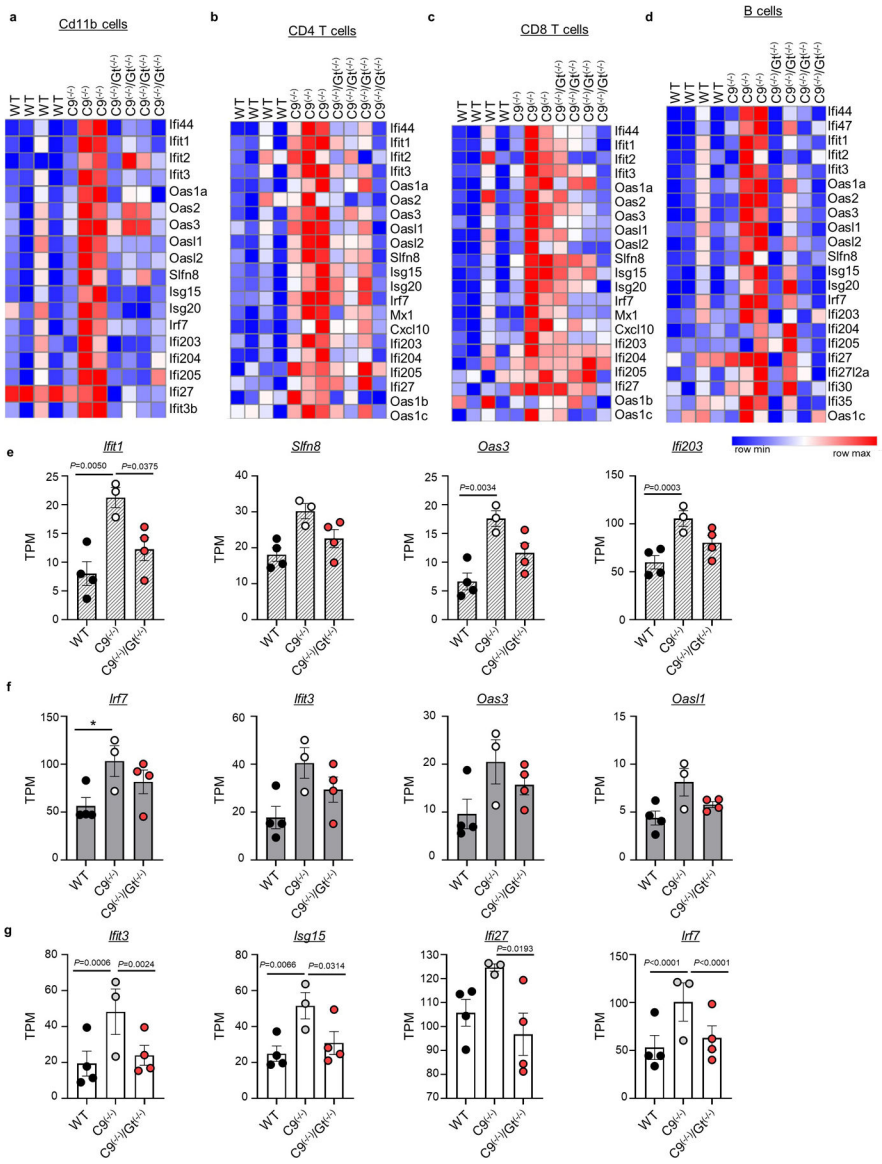


**Extended Data Fig. 6|. Deletion of STING mitigates the elevated type I IFN response signature in *C9orf72*$^{-/-}$ immune cells.**

**a.** Heat maps of ISGs from RNA-sequencing of isolated splenocyte populations from 3 month old animals. Cell types are indicated and included **a.** CD11b myeloid cells, **b.** CD4 T cells, **c.** CD8 T cells and **d.** B cells from wildtype (WT), *C9orf72* knockouts (C9$^{(-/-)}$) and *C9orf72*:STING double knockout (C9$^{(-/-)}$/Gt$^{(-/-)}$) mice. **e-g.** TPM values of indicated ISGs in **e.** CD4 T cells (WT n=4), *C9orf72* knockouts (C9$^{(-/-)}$n=3) and *C9orf72*:STING double knockout (C9$^{(-/-)}$/Gt$^{(-/-)}$n=4), **f.** CD8 T cells(WT n=4), *C9orf72* knockouts (C9$^{(-/-)}$n=3) and *C9orf72*:STING double knockout (C9$^{(-/-)}$/Gt$^{(-/-)}$n=4) and **g.** B cells (WT n=4), *C9orf72* knockouts (C9$^{(-/-)}$n=3) and *C9orf72*:STING double knockout (C9$^{(-/-)}$/Gt$^{(-/-)}$n=4). Deletion of STING showed marked rescue of the ISG expression across all cell types. **e-g.** Two-way ANOVA. **e-g.** Data are presented as mean values +/− SEM.

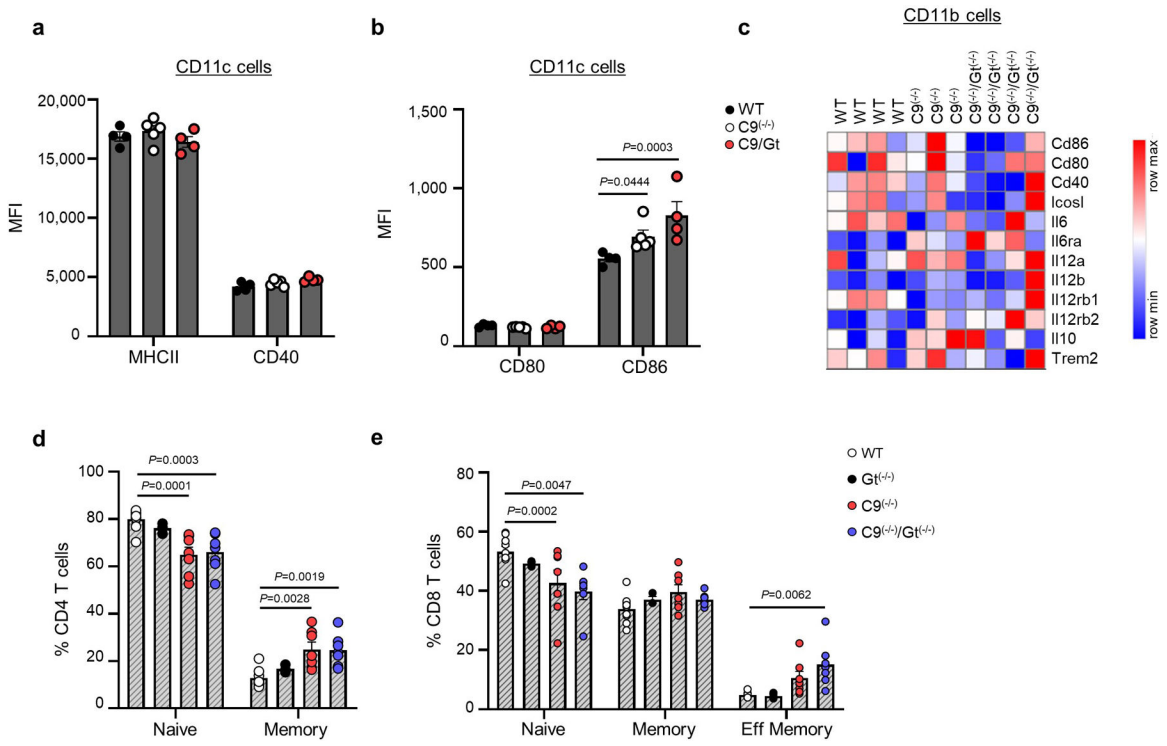


**Extended Data Fig. 7|. Activation markers of splenocyte populations in wildtype (WT), C9orf72$^{-/-}$ (C9$^{(-/-)}$) and STING knockout (Gt($^{-/-}$) mice.**

**a, b.** Flow cytometry of splenic CD11c co-stimulatory markers in 3-month old WT (n=4), C9$^{(-/-)}$ (n=5) and C9$^{(-/-)}$/Gt$^{(-/-)}$ (n=4) mice. **c.** RNA-sequencing of splenic CD11b cells in 3-month old WT (n=4), C9$^{(-/-)}$ (n=3) and C9$^{(-/-)}$/Gt$^{(-/-)}$ (n=4) mice. **d.** Flow cytometry of splenic CD4 T cells and **e.** CD8 T cells of 3-month old mice. One-way ANOVA. **a,b,d,e.** Data are presented as mean values +/− SEM.

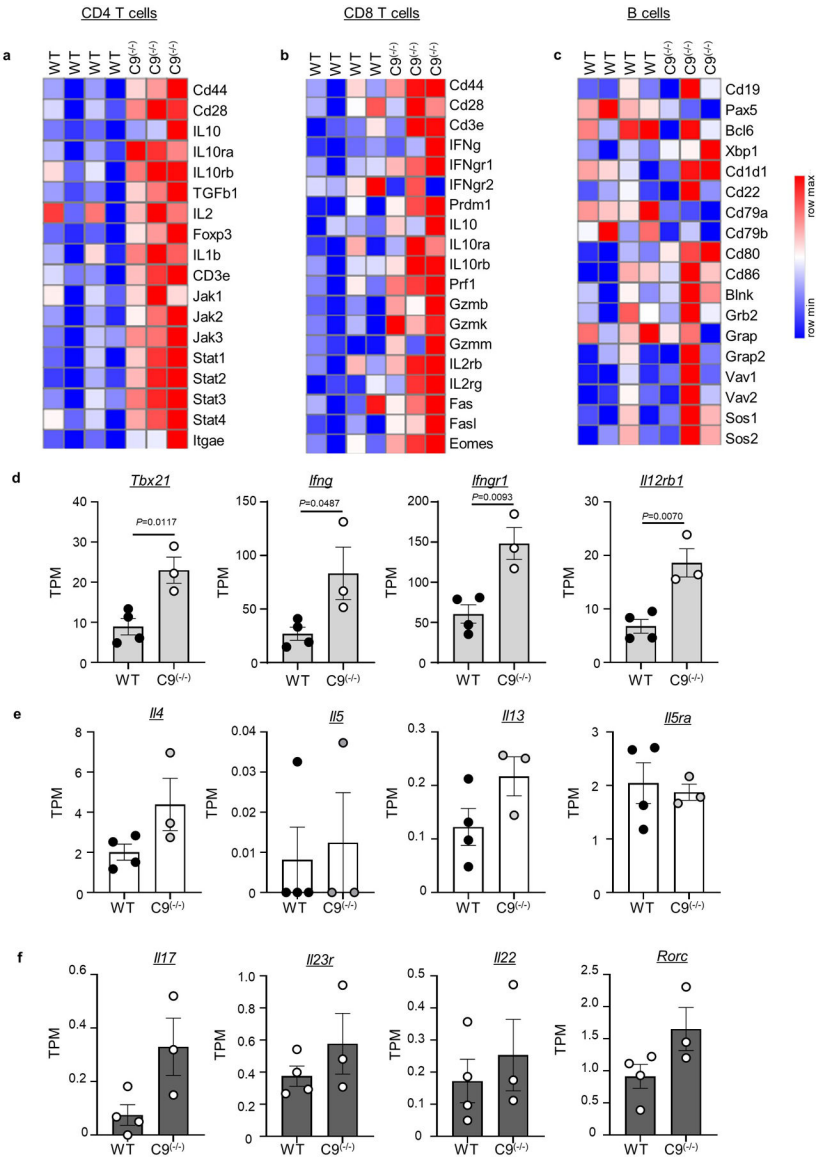


**Extended Data Fig. 8 |. *C9orf72*$^{-/-}$ T cells show increased activation and markers of Th1 polarization.**

Heat map of RNA-sequencing data from isolated CD4 T cells **(a)**, CD8 T cells **(b)**, and B cells **(c)** from spleens of 3 month old WT(n=4) and C9$^{(-/-)}$ (n=3) mice. Shown are markers of **d.** Th1 **e.** Th2 and **f.** Th17 polarization genes of CD4 T cells. Two-way ANOVA. **d-f.** Data are presented as mean values +/− SEM

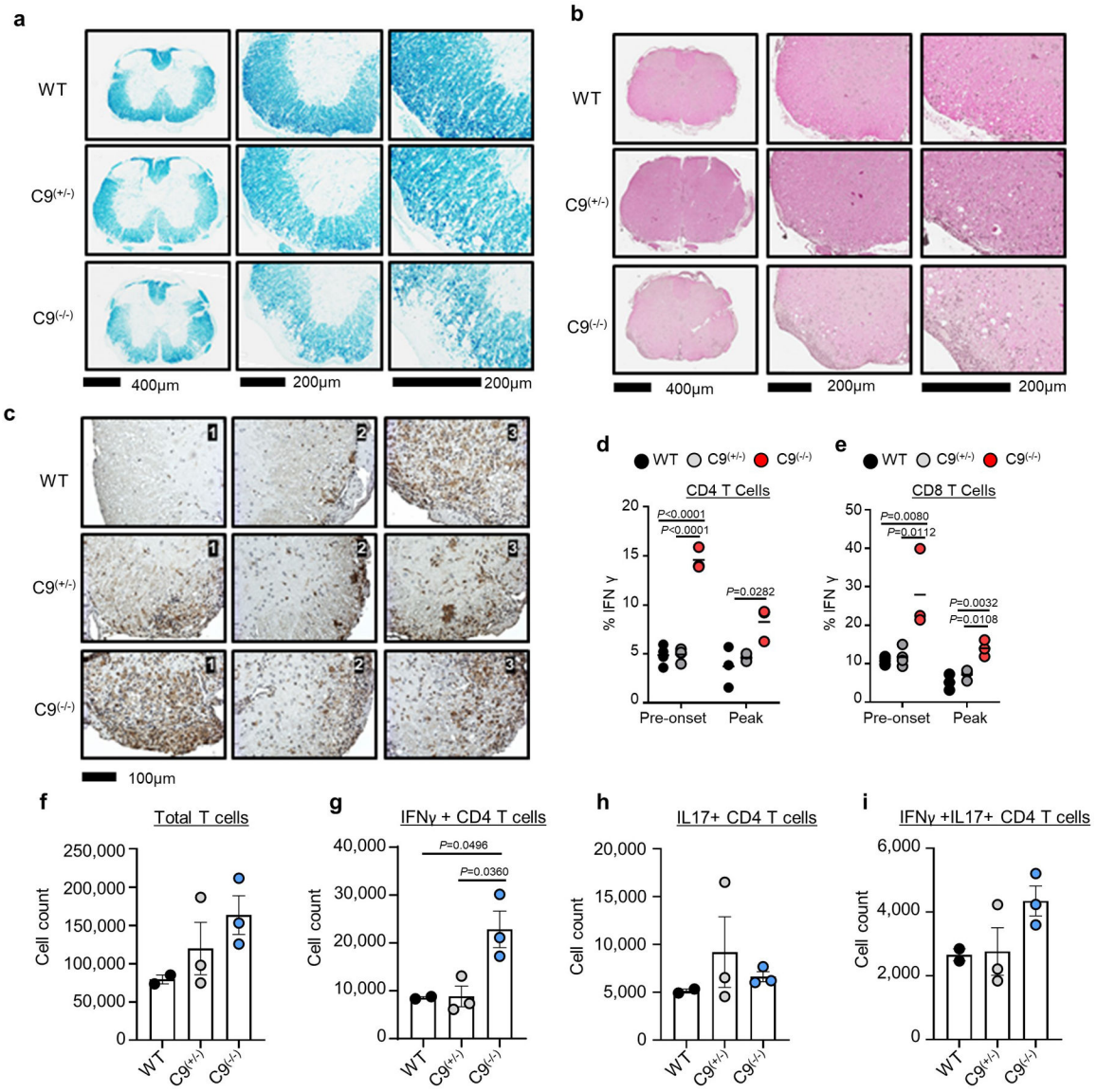


**Extended Data Fig. 9|. *C9orf72*$^{-/-}$ mice are more susceptible to EAE than wildtype mice and increased infiltration of Th1 polarized T cells into nervous tissue.**

**a.** Representative luxol fast blue (LFB) staining of spinal cord of WT (n=3), C9$^{(+/-)}$(n=3) and C9$^{(-/-)}$ (n=3) mice. **b.** Representative H&E staining of spinal cords from WT (n=3), C9$^{(+/-)}$ (n=3) and C9$^{(-/-)}$ (n=3) mice at end stage. **c.** Iba1 staining of spinal cord of indicated genotypes (n=3). **d.** Splenic C9$^{(-/-)}$ CD4 and **e.** CD8 T cells produce increased levels of IFNγ during pre-onset (day 9) (WT n=4, C9$^{(+/-)}$ n=4), C9$^{(-/-)}$ n=3 biologically independent samples) and peak (day 15) (WT n=3, C9$^{(+/-)}$ n=3, C9$^{(-/-)}$ n=3 biologically independent samples) of EAE **f.** Total number of CD3+ T cells **g.** IFNγ + CD4 T cells, **h.** IL17+ CD4 T cells and **i.** IFNγ+IL17+ CD4 T cells in whole brain of WT (n=2), C9$^{(+/-)}$ (n=3) and C9$^{(-/-)}$ (n=3) mice during peak (day 15) of disease. **f-i.** One-way ANOVA. **f-i.** Data are presented as mean values +/− SEM.

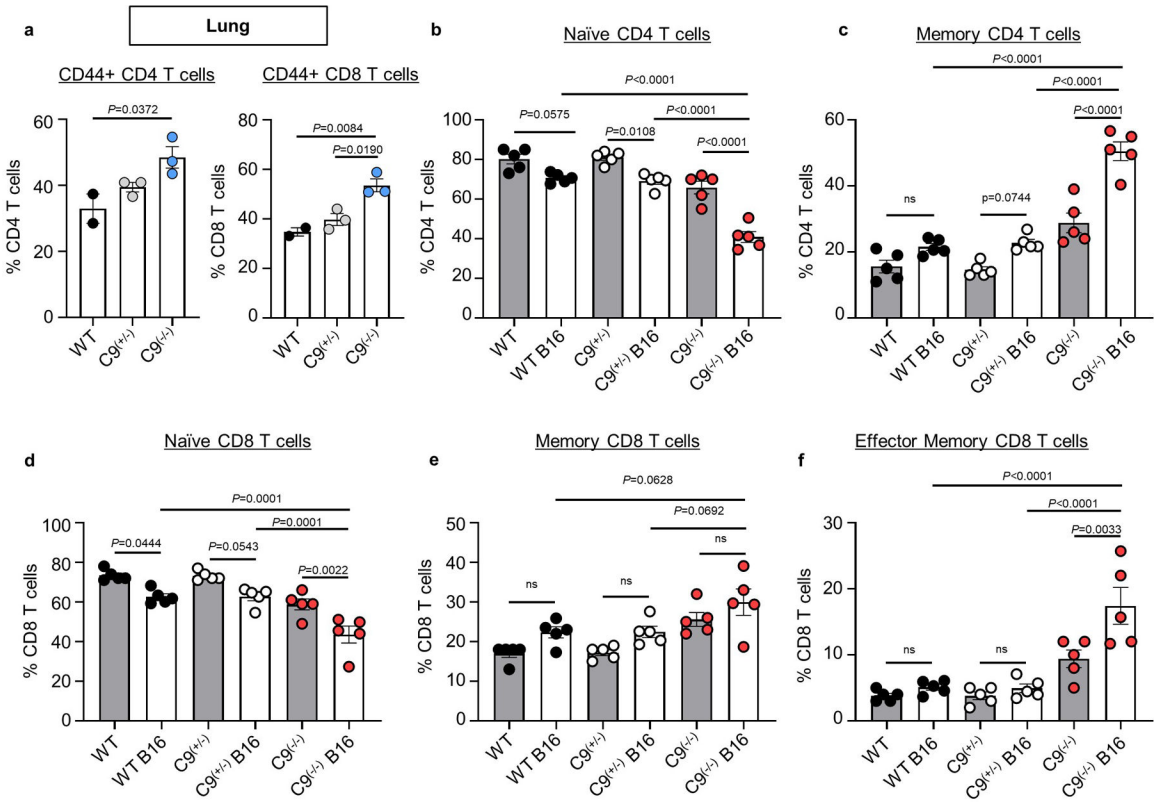


**Extended Data Fig. 10|. *C9orf72*$^{-/-}$ mice resistant to B16 melanoma tumors show an enhanced cytotoxic T cell response.**

**a.** Percent CD44+ CD4 T cells (left) and CD8 T cells (right) in the lung of WT (n=2), C9$^{(+/-)}$ (n=3) and C9$^{(-/-)}$ (n=3) mice day 14 of B16 melanoma challenge. **b.** Percent of naïve CD4 T cells and **c.** Memory CD4 T cells in the spleens of WT, C9$^{(+/-)}$ and C9$^{(-/-)}$ mice with and without B16 inoculation (n=5). **d.** Percent of naïve CD8 T cells, **e.** memory CD8 T cells and **f.** effector memory CD8 T cells in the spleens of wildtype, C9$^{(+/-)}$ and C9$^{(-/-)}$ mice with and without B16 inoculation (n=5). One-way ANOVA. Data are presented as mean values +/− SEM.

## Supplementary Material

Refer to Web version on PubMed Central for supplementary material.

## Acknowledgements

We thank R. Jeroen Pasterkamp for providing the *C9orf72*$^{fl/fl}$ mice, M. Vasquez for maintaining the animal colony, H. Maghzi for assisting with experimental autoimmune encephalitis, G. Martins for running the flow cytometry core and and M. Maniex for assistance with tissue collection. A.Y. is the recipient of a Ramón y Cajal fellowship from the Ministerio de Ciencia, Innovación y Universidades, Spain. This work was supported by NIH grant NS069669 (R.H.B), the Robert and Louise Schwab family; the Cedars-Sinai ALS Research Fund (R.H.B.), Arthritis Foundation AF2017-433570 (C.J), and NIH grant 1R21AI126368-01 (M.A.).

## References


1. Turner MR, Goldacre R, Ramagopalan S, Talbot K & Goldacre MJ Autoimmune disease preceding amyotrophic lateral sclerosis: an epidemiologic study. Neurology 81, 1222–1225, doi:10.1212/WNL.0b013e3182a6cc13 (2013). [PubMed: 23946298]
2. Miller ZA et al. TDP-43 frontotemporal lobar degeneration and autoimmune disease. Journal of neurology, neurosurgery, and psychiatry 84, 956–962, doi:10.1136/jnnp-2012-304644 (2013).
3. Miller ZA et al. Increased prevalence of autoimmune disease within C9 and FTD/MND cohorts: Completing the picture. Neurology(R) neuroimmunology & neuroinflammation 3, e301, doi:10.1212/NXI.0000000000000301 (2016). [PubMed: 27844039]
4. DeJesus-Hernandez M et al. Expanded GGGGCC hexanucleotide repeat in noncoding region of C9ORF72 causes chromosome 9p-linked FTD and ALS. Neuron 72, 245–256, doi:10.1016/j.neuron.2011.09.011 (2011). [PubMed: 21944778]
5. Renton AE et al. A hexanucleotide repeat expansion in C9ORF72 is the cause of chromosome 9p21-linked ALS-FTD. Neuron 72, 257–268, doi:10.1016/j.neuron.2011.09.010 (2011). [PubMed: 21944779]
6. Belzil VV et al. Reduced C9orf72 gene expression in c9FTD/ALS is caused by histone trimethylation, an epigenetic event detectable in blood. Acta Neuropathol 126, 895–905, doi:10.1007/s00401-013-1199-1 (2013). [PubMed: 24166615]
7. O'Rourke JG et al. C9orf72 is required for proper macrophage and microglial function in mice. Science 351, 1324–1329, doi:10.1126/science.aaf1064 (2016). [PubMed: 26989253]
8. Atanasio A et al. C9orf72 ablation causes immune dysregulation characterized by leukocyte expansion, autoantibody production, and glomerulonephropathy in mice. Scientific reports 6, 23204, doi:10.1038/srep23204 (2016). [PubMed: 26979938]
9. Burberry A et al. Loss-of-function mutations in the C9ORF72 mouse ortholog cause fatal autoimmune disease. Science translational medicine 8, 347ra393, doi:10.1126/scitranslmed.aaf6038 (2016).
10. Ganguly D, Haak S, Sisirak V & Reizis B The role of dendritic cells in autoimmunity. Nat Rev Immunol 13, 566–577, doi:10.1038/nri3477 (2013). [PubMed: 23827956]
11. Gardner A & Ruffell B Dendritic Cells and Cancer Immunity. Trends Immunol 37, 855–865, doi:10.1016/j.it.2016.09.006 (2016). [PubMed: 27793569]
12. Koppers M et al. C9orf72 ablation in mice does not cause motor neuron degeneration or motor deficits. Ann Neurol 78, 426–438, doi:10.1002/ana.24453 (2015). [PubMed: 26044557]
13. Abram CL, Roberge GL, Hu Y & Lowell CA Comparative analysis of the efficiency and specificity of myeloid-Cre deleting strains using ROSA-EYFP reporter mice. Journal of immunological methods 408, 89–100, doi:10.1016/j.jim.2014.05.009 (2014). [PubMed: 24857755]
14. Zhang X et al. Cyclic GMP-AMP containing mixed phosphodiester linkages is an endogenous high-affinity ligand for STING. Mol Cell 51, 226–235, doi:10.1016/j.molcel.2013.05.022 (2013). [PubMed: 23747010]
15. Konno H, Konno K & Barber GN Cyclic dinucleotides trigger ULK1 (ATG1) phosphorylation of STING to prevent sustained innate immune signaling. Cell 155, 688–698, doi:10.1016/j.cell.2013.09.049 (2013). [PubMed: 24119841]
16. Gonugunta VK et al. Trafficking-Mediated STING Degradation Requires Sorting to Acidified Endolysosomes and Can Be Targeted to Enhance Anti-tumor Response. Cell reports 21, 3234–3242, doi:10.1016/j.celrep.2017.11.061 (2017). [PubMed: 29241549]
17. Prabakaran T et al. Attenuation of cGAS-STING signaling is mediated by a p62/SQSTM1-dependent autophagy pathway activated by TBK1. The EMBO journal 37, doi:10.15252/embj.201797858 (2018).
18. Nassif M, Woehlbier U & Manque PA The Enigmatic Role of C9ORF72 in Autophagy. Front Neurosci 11, 442, doi:10.3389/fnins.2017.00442 (2017). [PubMed: 28824365]
19. Gui X et al. Autophagy induction via STING trafficking is a primordial function of the cGAS pathway. Nature 567, 262–266, doi:10.1038/s41586-019-1006-9 (2019). [PubMed: 30842662]
20. Haag SM et al. Targeting STING with covalent small-molecule inhibitors. Nature 559, 269–273, doi:10.1038/s41586-018-0287-8 (2018). [PubMed: 29973723]

21. Sharma S et al. Suppression of systemic autoimmunity by the innate immune adaptor STING. Proceedings of the National Academy of Sciences of the United States of America 112, E710–717, doi:10.1073/pnas.1420217112 (2015). [PubMed: 25646421]
22. McAlpine W et al. Excessive endosomal TLR signaling causes inflammatory disease in mice with defective SMCR8-WDR41-C9ORF72 complex function. Proceedings of the National Academy of Sciences of the United States of America 115, E11523–E11531, doi:10.1073/pnas.1814753115 (2018). [PubMed: 30442666]
23. Huber JP & Farrar JD Regulation of effector and memory T-cell functions by type I interferon. Immunology 132, 466–474, doi:10.1111/j.1365-2567.2011.03412.x (2011). [PubMed: 21320124]
24. Gall A et al. Autoimmunity initiates in nonhematopoietic cells and progresses via lymphocytes in an interferon-dependent autoimmune disease. Immunity 36, 120–131, doi:10.1016/j.immuni.2011.11.018 (2012). [PubMed: 22284419]
25. O'Connor RA et al. Cutting edge: Th1 cells facilitate the entry of Th17 cells to the central nervous system during experimental autoimmune encephalomyelitis. Journal of immunology 181, 3750–3754, doi:10.4049/jimmunol.181.6.3750 (2008).
26. Ismail A et al. Concurrence of multiple sclerosis and amyotrophic lateral sclerosis in patients with hexanucleotide repeat expansions of C9ORF72. Journal of neurology, neurosurgery, and psychiatry 84, 79–87, doi:10.1136/jnnp-2012-303326 (2013).
27. Lemos H et al. Activation of the STING adaptor attenuates experimental autoimmune encephalitis. Journal of immunology 192, 5571–5578, doi:10.4049/jimmunol.1303258 (2014).
28. Gibson SB et al. Population-based risks for cancer in patients with ALS. Neurology 87, 289–294, doi:10.1212/WNL.0000000000002757 (2016). [PubMed: 27170569]
29. Woo SR et al. STING-dependent cytosolic DNA sensing mediates innate immune recognition of immunogenic tumors. Immunity 41, 830–842, doi:10.1016/j.immuni.2014.10.017 (2014). [PubMed: 25517615]
30. Prudencio M et al. Distinct brain transcriptome profiles in C9orf72-associated and sporadic ALS. Nat Neurosci 18, 1175–1182, doi:10.1038/nn.4065 (2015). [PubMed: 26192745]
31. Sliter DA et al. Parkin and PINK1 mitigate STING-induced inflammation. Nature 561, 258–262, doi:10.1038/s41586-018-0448-9 (2018). [PubMed: 30135585]
32. Xiao Y et al. The kinase TBK1 functions in dendritic cells to regulate T cell homeostasis, autoimmunity, and antitumor immunity. The Journal of experimental medicine 214, 1493–1507, doi:10.1084/jem.20161524 (2017). [PubMed: 28356390]

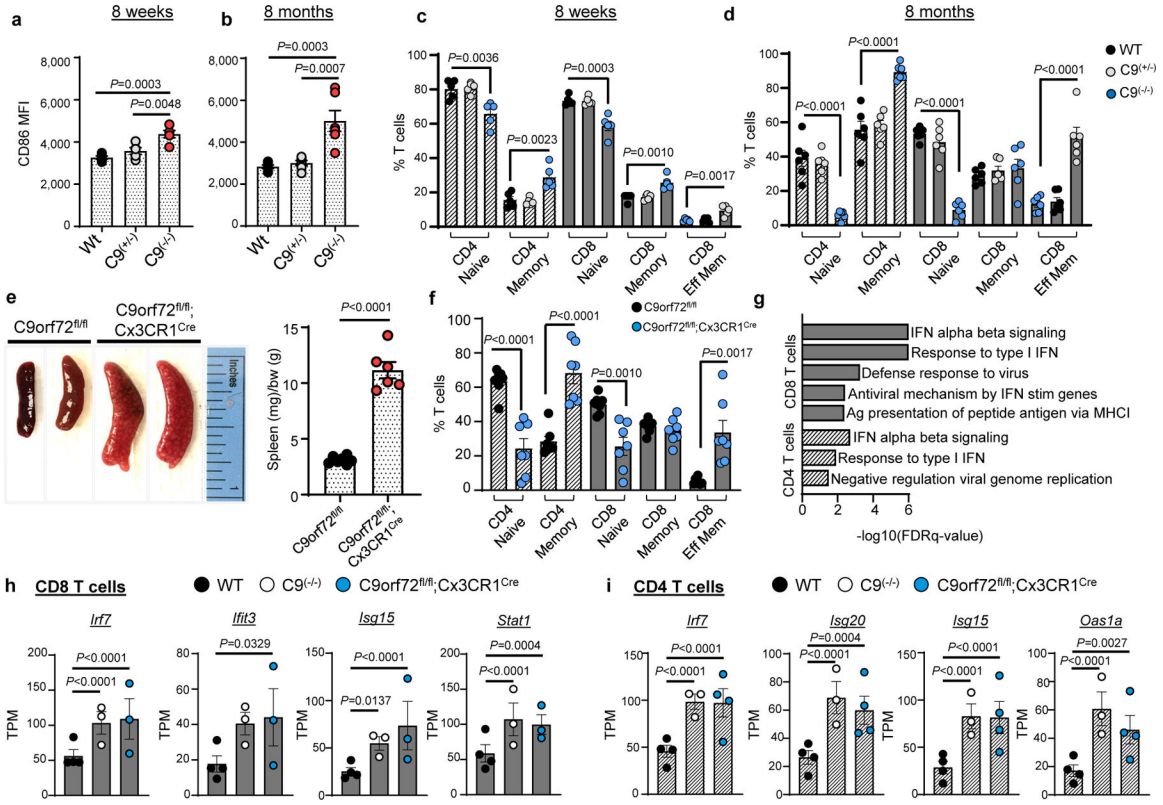


**Fig 1. |. Dendritic cell development and T cell activation in young and aged *C9orf72*$^{-/-}$ mice.**

**a**. Mean fluorescent intensity (MFI) of CD86 in CD11c+ splenic dendritic cells in young (n=5) and (**b**) aged mice (n=6). **c.** Flow cytometric analysis of naïve (CD62L+), memory (CD62L+, CD44+) and effector memory (CD44+) CD4 T cells and CD8 T cells for 8 week (n=5) and **d.** 8 month old animals (n=6). **e.** Gross images of splenomegaly in *C9orf72-Cx3cr1*$^{Cre}$ mice at 5 months (left). Spleen weights (mg) normalized to body weight (g) at 5 months (right) (n=7). **f.** C9orf72-Cx3cr1$^{Cre}$ mice have decreased naïve CD4 and CD8 T cells with an increase in CD4 memory and CD8 effector memory T cells (n=7). **g.** Gene set enrichment analysis (GSEA) of significantly upregulated pathways in CD8 T cells (grey) and CD4 T cells (striped) of C9orf72-Cx3cr1$^{Cre}$ mice vs wild-type (WT) at 3 months (FDR < 0.05) (n=4). **h,i.** TPM values from RNA seq showing non-cell autonomous elevation of interferon signature genes (ISGs) in CD8 (WT n=4, C9$^{(-/-)}$ n=3, C9orf72$^{fl/fl}$;Cx3CR1$^{Cre}$ n=3) and CD4 T cells (WT n=4, C9$^{(-/-)}$ n=3, C9orf72$^{fl/fl}$;Cx3CR1$^{Cre}$ n=4) in C9orf72-Cx3cr1$^{Cre}$ mice. **a-d, f.** One-way ANOVA, **e.** Unpaired, two tailed Students t-test. **h,i.** Two-way ANOVA. **a-f,h,i.** Data are presented as mean values +/− SEM. Each dot represents one mouse.

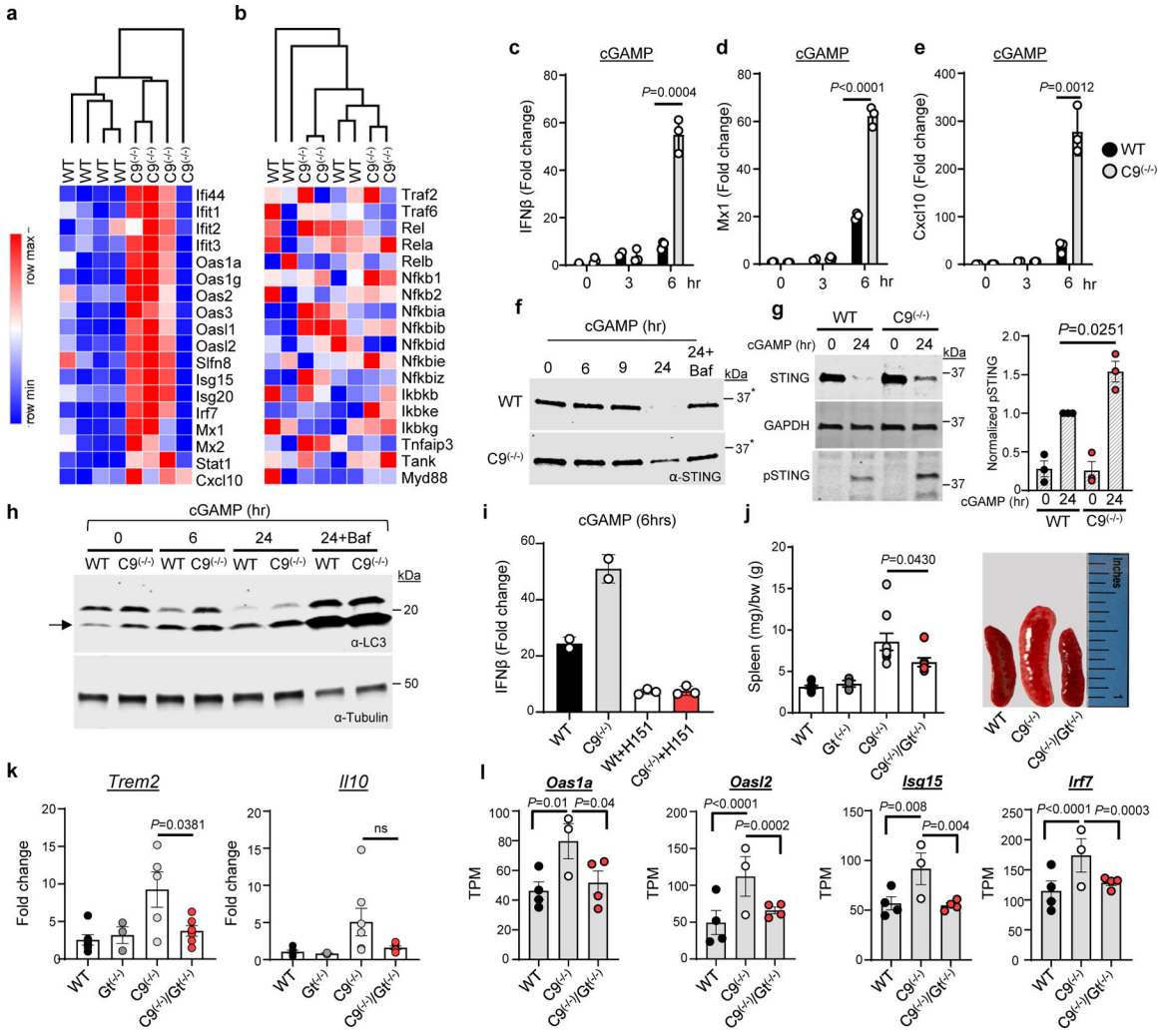


**Fig 2. |. Loss of *C9orf72* in myeloid cells drives increased type I interferon production through STING.**

Heat map (max-min normalized) of IFN-response **a.** or NF-kB-response genes **b.** in C9$^{(-/-)}$ vs. WT splenic cDCs via RNA-seq. **c.** qRT-PCR of IFNβ, **d.** Mx1 and **e.** Cxcl10 in BMDMs of WT and C9$^{(-/-)}$ mice following cGAMP (5μg/ml) stimulation (technical replicates representative of 4 biological replicates). **f.** Western blot of BMDMs stimulated with cGAMP (10μg/ml) for 0, 6, 9, 24, or 24 hours+Bafilomycin showing delayed STING degradation in C9$^{(-/-)}$ vs WT (representative of 4 experiments). *Molecular weight marker visualized (see Sup.Fig.1). **g.** Western blot of phospho-365 STING at (0h) vs. overnight (24h) cGAMP (10μg/ml) treatment on WT vs C9$^{(-/-)}$ BMDMs (left). Quantification of pSTING (right) from n=3 biological replicate experiments. **h.** BMDMs stimulated with cGAMP (10μg/ml) for 0, 6, 24, or 24 hours + Bafilomycin showing LC3-II (top blot, arrow) in WT vs C9$^{(-/-)}$ BMDM, with tubulin loading control (bottom blot) (representative of 4 biological replicates). **i.** qRT-PCR of IFNβ in BMDMs for WT and C9$^{(-/-)}$ with and without STING antagonist H151 (1μM) following cGAMP stimulation (technical replicates representative of 3 biological replicates). **j.** Spleen weight (mg) normalized to body weight (g) at 8–10 weeks (n=7) (left) and gross representative images (right). **k.** qRT-PCR of Trem2

and IL10 in total splenocytes of WT (n=6), $Gt^{(-/-)}$ (n=3), $C9^{(-/-)}$ (n=5) and $C9^{(-/-)}$:$Gt^{(-/-)}$ (n=6) mice**. l.** RNA-seq of interferon response gene expression from splenic CD11b+ cells in 3 month old WT (n=4), $C9^{(-/-)}$ (n=3), and $C9^{(-/-)}$/$Gt^{(-/-)}$ mice (n=4). Two-way ANOVA. **c-e,k.** Unpaired, two tailed Students t-test. **i,j,l.** One-way ANOVA. **e-g,k.** Data are presented as mean values +/− SD. **i,l-m.** Data are presented as mean values +/− SEM. **g,j-l.** Each dot represents one mouse. For gel source data, see Supplementary Figure 1.

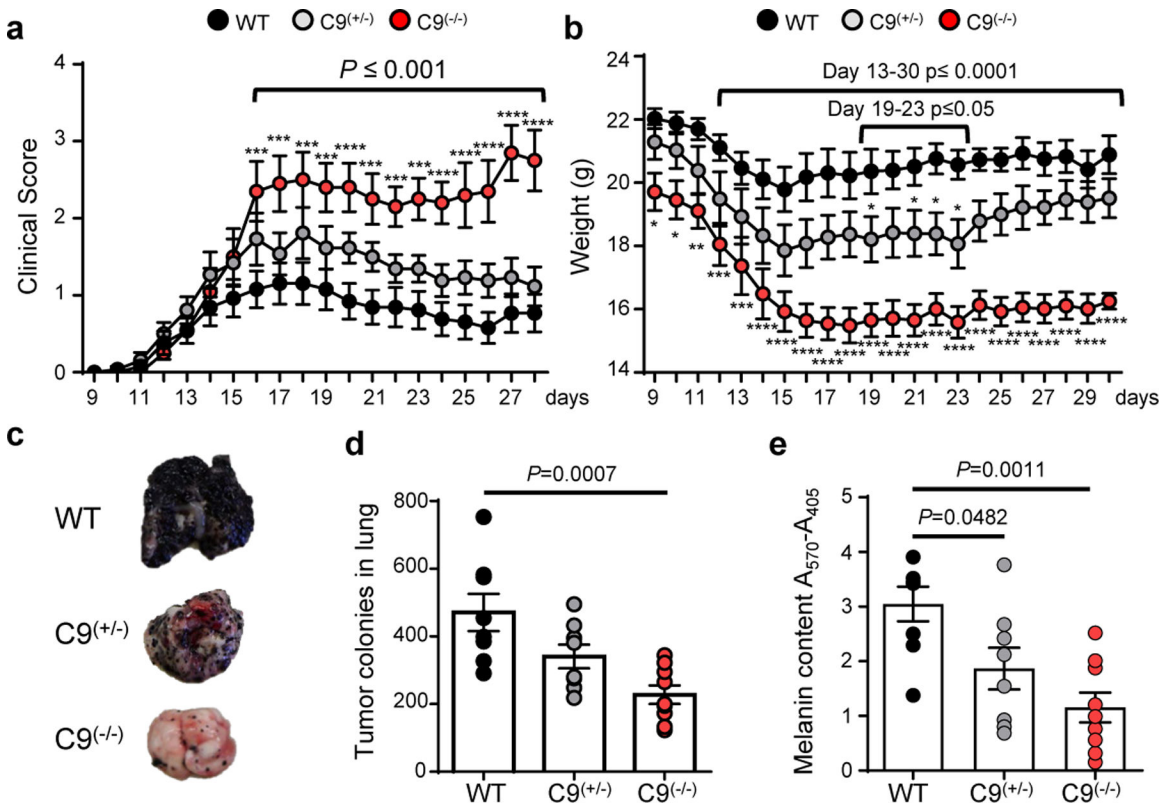


**Fig 3. |. *C9orf72*$^{-/-}$ mice are more susceptible to experimental autoimmune encephalomyelitis (EAE) and have increased antitumor immunity.**

**a.** EAE clinical score and **b.** Weight (g) over the course of EAE on WT (n=13), C9$^{(+/-)}$ (n=13), C9$^{(-/-)}$ (n=10) mice. **c.** Representative images of lungs from WT, C9$^{(+/-)}$ and C9$^{(-/-)}$ mice 14 days after B16 inoculation. **d.** C9$^{(-/-)}$ mice have decreased number of tumor colonies (WT n=8, C9$^{(+/-)}$ n=8, C9$^{(-/-)}$ n=9) and **e.** melanin content after inoculation with B16 melanoma cells for 14 days (WT n=6, C9$^{(+/-)}$ n=8, C9$^{(-/-)}$ n=9). One-way ANOVA. **a, b, d, and e.** Data are presented as mean values +/− SEM. **d,e.** Each dot represents one mouse.

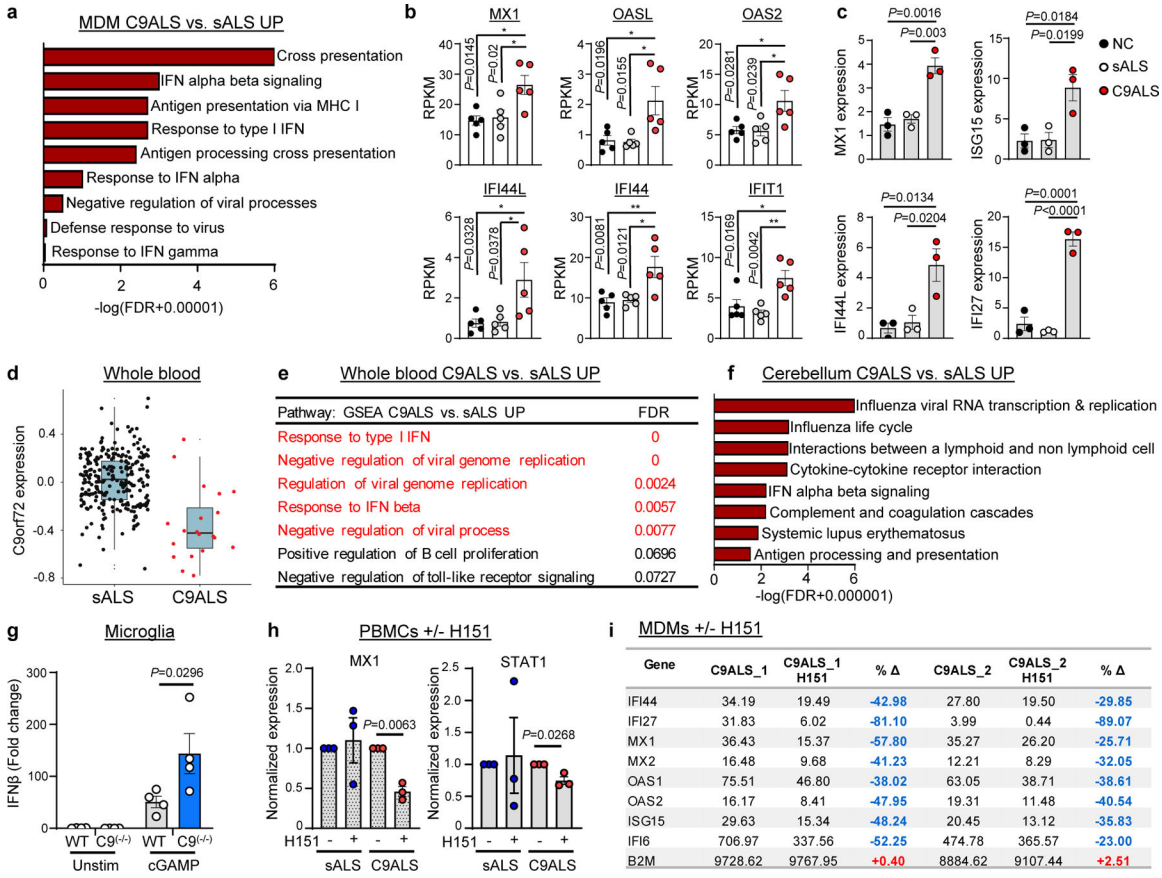


**Fig 4. |. *C9orf72* repeat expansion ALS patients have an enhanced type I IFN signature in peripheral myeloid cells that can be suppressed by a STING antagonist.**

**a.** GSEA of RNA-seq from MDM between C9ALS (n=5) vs. sALS (n=5) patients (FDR < 0.05). **b.** RPKM of type I IFN stimulated gene expression in C9ALS MDMs compared to sALS and normal controls (NC) (n=5). One-way ANOVA. **c.** qRT-PCR validation of IFN stimulated genes in (**b**) (n=3). One-way ANOVA. **d.** Whole blood RNA-seq from C9ALS patients (n=20) showing decreased C9orf72 expression compared to sALS patients (n=259) sALS (left box): n=259, min = −0.722, max = 0.697. Whiskers = [−0.562, 0.625], box = [−0.147, 0.174], median = 0.0214. C9ALS (right box), n=20, min = −0.779, max=0.355, Whiskers = [−0.779, 0.211], Box = [−0.551, −0.215], median = −0.425. **e.** Upregulated pathways from RNA-seq of whole blood between C9ALS vs sALS (FDR < 0.05). **f.** Upregulated inflammatory pathways of cerebellar tissue between C9ALS (n=8) and sALS (n=10) patients (FDR < 0.05). **g.** qRT-PCR of IFNβ production from microglia isolated from WT (n=4) and C9orf72$^{-/-}$ (n=4) mouse brain after cGAMP stimulation. Unpaired, one-tailed Student's t-test. **h.** qRT-PCR of ISGs MX1 and STAT1 in sALS and C9ALS patients PBMCs with and without H151 STING inhibitor (1μM) (n=3). Paired, one-tailed Students t-test. **i.** Table of TPM values of indicated interferon stimulated genes from RNA-sequencing of MDM's from two *C9orf72* patients with and without H151 STING inhibitor (6 hours). Blue=percent decreased, red=percent increased. **b, c, g, and h.** Data are presented as mean values +/− SEM. Each dot represents one sample.